Cellulose
https://doi.org/10.1007/s10570-024-06169-0

ORIGINAL RESEARCH

Synergistic effect of "methyl cellulose-dextran" on oral curcumin delivery via casein nanomicelle: fabrication, characterization, and cancer therapeutic efficacy assessment

Samia F. Aboushoushah · Sana F. Abaza · Nihal S. Elbialy · Noha Mohamed

Received: 18 May 2024 / Accepted: 10 September 2024

Abstract A casein-methyl cellulose nanocomplex, loaded with curcumin and coated with dextran (DX-CasCur-MC), is designed to enhance curcumin's oral delivery and inhibit cancer growth. Its physicochemical properties reveal chemical bonding between protein and polysaccharides, transforming curcumin from crystalline into amorphous state to improve water solubility. The encapsulation efficiency of curcumin reaches 92%, and its release profile in physiological and tumor microenvironments exhibits controlled and sustained release. In vitro studies confirm the significant therapeutic efficacy of DX-CasCur-MC in inducing cancer cell death and DNA damage compared to free curcumin. The effectiveness of DX-CasCur-MC for oral drug delivery is validated in simulated gastrointestinal fluids, with 23 and 69% release in gastric and intestinal fluids, respectively. In vivo studies demonstrate a significant reduction in tumor volume in mice treated with DX-CasCur-MC compared to those treated with free curcumin or untreated, confirming DX-CasCur-MC's ability to improve curcumin's pharmacological properties and inhibit tumor growth via repeated oral administration. The conjugation of the two polysaccharides with the hydrocolloidal casein nanomicelles improves the nanocomplexes stability, making DX-CasCur-MC a promising natural candidate for oral curcumin delivery with a significant cancer therapeutic efficacy.

Keywords Curcumin-casein-methyl cellulose-dextran nanocomplex · Cancer · Oral drug delivery

Supplementary Information The online version contains supplementary material available at https://doi.org/10.1007/s10570-024-06169-0.

S. F. Aboushoushah · N. S. Elbialy (✉)
Medical Physics Program, Department of Physics, Faculty of Sciences, King Abdulaziz University, 21589 Jeddah, Saudi Arabia
e-mail: nsmohamad@kau.edu.sa; n_elbialy@cu.edu.eg

S. F. Aboushoushah
e-mail: saboushoushah@kau.edu.sa

S. F. Abaza
Department of Physics, Faculty of Sciences, King Abdulaziz University, 21589 Jeddah, Saudi Arabia
e-mail: sabaza@kau.edu.sa

N. Mohamed
Biophysics Department, Faculty of Science, Cairo University, Giza 12613, Egypt
e-mail: nmsayed@sci.cu.edu.eg

Introduction

Cancer stands as the second leading cause of global mortality (Bray et al. 2018; Siegel et al. 2020), with the incidence and fatality rates painting a grim picture of the limited effectiveness of traditional treatment modalities. The primary cancer treatments including surgery, radiotherapy, and chemotherapy are marred by severe side effects and organ toxicity, significantly impacting the quality of life for those battling cancer.

Published online: 13 September 2024

It is well known that most cancer patients receive chemotherapeutics owing to their efficacy against various cancer types with improving patient survival rates. Unfortunately, they are accompanied not only by severe side effects but also by the development of multidrug resistance (Mansoori et al. 2017). Furthermore, recent studies highlight that the resistance to radiotherapy, chemotherapy, and immunotherapy can be linked to specific biological markers, indicating a more complex interplay of the tumor immune microenvironment in treatment failures (He et al. 2023). Therefore, the pursuit of either an adjunct to current therapies or the creation of a safe, more effective alternative is imperative. This attempt aims to reduce mortality rates and improve the overall quality of life for cancer patients (Yallapu et al. 2013).

Numerous innovative cancer treatment strategies have emerged recently, with options ranging from advanced drug delivery systems and photothermal therapy to natural drugs and nutraceuticals. These include exploring the potential of nanoscale coordination polymers, advancing immunotherapy using messenger RNA, developing efficient organic sonosensitizers for sonodynamic therapy, and advancements in molecular genetics (Kasi et al. 2016; Zhang et al. 2022; Liu et al. 2022a, b; Li et al. 2022b; Chen et al. 2023; Deb et al. 2024).

Natural drugs and nutraceuticals have garnered particular attention as promising alternatives to traditional chemotherapy, appealing to both the scientific community and cancer patients. In the USA, approximately 50–60% of cancer patients turn to nutraceuticals as substitutes for conventional chemotherapeutics (Yadav et al. 2020; Pan et al. 2022). Bioactive compounds such as curcumin, lycopene, royal jelly, and resveratrol have demonstrated potent anticancer properties (Naksuriya et al. 2014; Rauf et al. 2018; Pradhan et al. 2021; Xu et al. 2023). There has been particular enthusiasm surrounding the therapeutic efficacy of curcumin against various types of cancer.

Curcumin has evolved from its role as a mere adjunct in therapy to becoming a potent alternative in the treatment of various types of cancer. Derived from Curcuma longa, curcumin is a natural polyphenolic compound showcasing diverse pharmacological properties, rendering it valuable as an antioxidant, anti-inflammatory agent, and anticancer agent (Fan et al. 2018; Gao et al. 2022). Despite numerous clinical trials affirming the safety and efficacy of curcumin against cancer (Zoi et al. 2021), its medical utility is still under investigation. Hindrances include poor water solubility, low pharmacodynamic profile, limited intestinal permeability, and rapid metabolism and clearance, collectively contributing to its suboptimal oral bioavailability (Anand et al. 2007).

The creation of a nano-drug delivery system stands out as a promising approach to overcome the aforementioned challenges (He et al. 2021; Rajendran et al. 2024). Despite various nano-drug delivery systems being explored to enhance curcumin solubility, stability, and bioavailability (Zheng et al. 2017; Araiza-Calahorra et al. 2018), a particularly intriguing avenue is the incorporation of food-derived components, specifically proteins and polysaccharides. The biocompatibility, biodegradability, immune-boasting effect, and functionality of proteins and polysaccharides make them ideal for various medical applications, particularly in effectively encapsulating therapeutic agents (Fan et al. 2015; Xiaolong 2023; Yi et al. 2023; Shen et al. 2023; Zhang et al. 2024).

Casein, a high-quality milk protein comprising αs1, αs2, β, and κ casein components, exhibits a linear amphiphilic nature (Elzoghby et al. 2011). Utilizing its high bioavailability and non-immunogenicity properties, casein serves as an effective nano-drug delivery system. Self-assembly of casein leads to micelles formation with a hydrophobic core and hydrophilic shell, facilitating the encapsulation of curcumin (Chang et al. 2017). The encapsulation in casein micelles involves physical embedding, covalent bonding, and electrostatic interaction (Liu et al. 2020). Despite casein's susceptibility to low water resistance and weak mechanical strength, its high content of polar groups—such as hydroxyl, carboxyl, and amino—allows for conjugation with other materials (Fan et al. 2015). Advances in protein modifications result in a hybrid nanomaterial with enhanced properties. The application of casein as an oral nanocarrier can be expanded through conjugation with biopolymers like polysaccharides.

Recent attention in the field of cancer oral drug delivery has focused on the synergistic conjugation of proteins and polysaccharides, leveraging the complementary strengths, and addressing the weaknesses of each. Whereas proteins are efficient at producing small emulsion droplets, but are relatively unstable in environmental stimuli, polysaccharides are stable in such environments, but have moderately low

emulsifying activity (Sun et al. 2022). The formation of protein-polysaccharide complexes provides cost-effective, renewable, soluble, bioavailable, and biodegradable formulations. The merging of numerous polysaccharides with casein, either within its structure or as a shell, enhances casein's role as an oral delivery system for curcumin while addressing challenges associated with using casein micelles individually.

This conjugation is essential to address the inherent instability of casein micelles, rapid drug leakage, and the vulnerability of casein in the gastric environment, ultimately leading to degradation. Nano-conjugation of proteins with polysaccharides acts as a protective shield, safeguarding casein micelles and the encapsulated drug from enzymatic degradation. This nano-conjugation ensures controlled drug release in the gastrointestinal tract, establishing its utility as an oral drug delivery system (Chang et al. 2017; Alavi et al. 2018) Currently, researchers are directing their focus towards the oral delivery route, given its convenience and widespread acceptance among most cancer patients.

Various polymeric materials, including chitosan (Jiang et al. 2012; Ding et al. 2019), hyaluronic acid (Choi et al. 2012; Li et al. 2014), and polyethylene glycol (Hao et al. 2021), have been employed as block copolymers to modify and coat casein micelles, resulting in heightened stability and bioavailability for loaded drugs. Cellulose in the native, mercerized, or regenerated (e.g., rayon) form offers the advantages of being non-toxic, biocompatible, and biodegradable, along with excellent physicochemical properties. Cellulose derivatives like methyl cellulose and carboxymethyl cellulose have garnered attention for their ability to form diverse nanostructures (Klemm et al. 2021; Ho and Leo 2021), or combine with other nanomaterials (Prusty and Swain 2019; Gupta et al. 2019). For instance, a previous study demonstrated the conjugation of Fe_3O_4 with curcumin-loaded cellulose nanocarriers for in vitro treatment of colon cancer (Low et al. 2019).

The polysaccharide dextran, biologically synthesized by microbes, forms poly-D-glucoside with intricate branching. Dextran's capacity to form complexes with diverse biomaterials enhances its suitability for drug delivery in pulmonary, ocular, and nasal applications (Vandamme et al. 2002). The nanoconjugation of curcumin, such as curcumin-γ-hydroxypropyl cyclodextrin, has demonstrated successful gene therapy delivery to cancer cells compared to conventional drugs (Popat et al. 2014). Remarkably, various in vivo xenograft mouse models have shown that conjugating dextran with carboxymethyl cellulose significantly enhances the effectiveness of cancer cell death (Posey et al. 2005; Chau et al. 2006; Schneible et al. 2021).

The objective of the present study is to fabricate, characterize, and assess the potential of the proposed nanoplatform (dextran-casein-methyl cellulose) for the oral delivery of curcumin. The optimized properties of this nanocomplex aim to fortify curcumin in the gastrointestinal tract, enhance its oral bioavailability and impede cancer cell growth by inducing DNA damage and arresting cell cycle progression.

Materials and methods

Materials

Sodium caseinate from bovine milk (Molecular weight = 314 g/mol), curcumin (> 94% curcuminoid with a molecular weight 368.38), methylcellulose (low molecular weight 10–20 kDa), dextran sulfate (molecular weight 5 kDa), dimethyl sulfoxide (DMSO), phosphate buffered saline (PBS) and Dextran sulfate sodium salt from leuconostoc spp, M_r 5000 Da (Sigma–Aldrich -USA).

Methods

Curcumin encapsulation in casein-methyl cellulose nanoparticles

To synthesize curcumin-loaded casein methyl cellulose nanoparticles (CasCur-MC), methyl cellulose (MC) solution was prepared by dissolving 20 mg MC in distilled water (10 ml) and stirred until the formation of a clear solution. Similarly, sodium caseinate solution was prepared by dissolving sodium caseinate (20 mg) in distilled water (10 ml). The curcumin solution was prepared by dissolving curcumin (20 mg) in 1 ml of 0.1% dimethyl sulfoxide (DMSO). For curcumin loading, sodium caseinate solution was then mixed with the curcumin solution followed by 30 min stirring. Then, MC solution was added to casein loaded nanoparticles (CasCur) and stirred until the formation of homogenous solution (CasCur-MC). By

using a centrifuge (at 10,000 rpm/30 min), CasCur-MC solution was separated from unloaded curcumin which was further quantified (using spectrofluorometer at $\lambda_{excitation} = 425$ nm and $\lambda_{emission} = 530$ nm) to evaluate the amount of encapsulated curcumin in casein micelles.

Dextran sulfate coating

To prepare dextran sulfate (DX) solution, 0.1 g of dextran sulfate was dissolved in 10 ml distilled water (10 ml) and stirred vigorously until complete dissolution. Then, DX solution (1 ml) was dropped on CasCur-MC solution (10 ml) forming DX-CasCur-MC solution. To discard the excess dextran, DX-CasCur-MC solution was centrifuged (10,000 rpm/30 min), then the precipitated nanocomplex was resuspended in distilled water.

Encapsulation efficiency

Encapsulation efficiency (EE) determines the ratio of the amount of curcumin encapsulated in casein nanomicelles to the amount of curcumin initially used. Drug encapsulation efficiency by casein methyl cellulose nanoparticles (CasCur-MC) was calculated by:

$$\text{EE}\,(\%) = \frac{\textit{initial amount of Cur} - \textit{unloaded Cur in supernant}}{\textit{initial amount of Cur}} \times 100$$

It should be noted that unloaded curcumin was previously quantified by a calibration curve (concentrations *vs* fluorescence intensity) and spectrofluorometer.

Measurements of physicochemical properties of nanocomplex

Transmission electron microscopy Transmission electron microscopy (TEM) was used for imaging the morphology of the curcumin loaded nanoparticles (DX-CasCur-MC) and the unloaded nanoparticles (Cas-MC). Phosphotungstic acid staining was applied to enhance visualization [JEM 1230, Joel, Japan].

Fluorescence measurement The fluorescence spectra of Cur, Cas-MC, DX-Cas-MC, and DX-CasCur-MC solutions were recorded using a spectrofluorometer at emission wavelength 341 nm for measuring protein and 550 nm for measuring curcumin (RF 5301pc; Shimadzu, Japan).

Hydrodynamic size distribution and zeta potential measurements Using a Nano-Zetasizer, particle size distribution of Cas-MC and DX-CasCur-MC, as well as the zeta potential of the synthesized Cas-MC, CasCur-MC, and DX-CasCur-MC, were measured in triplicate at an ambient temperature (ZS90—Malvern Panalytical, UK).

Fourier transform infrared measurements Fourier transform infrared (FTIR) spectra for Cur, Cas-MC, CasCur-MC, and DX-CasCur-MC in the solid form were measured using FTIR spectrometer (R-4100 type A -Basic Vector, Germany). Measurements were conducted over 4000–400 cm^{-1} range.

X-ray diffraction X-ray diffraction (XRD) patterns of Cas-MC, CasCur-MC, and DX-CasCur-MC in the solid form were determined by an X-ray diffractometer (X-ray Diffractometer- Malvern Panalytical) in the range from 2° to 100°. The instrument was set at a 0.02° scanning step with a speed of 0.1 s/step.

Thermogravimetric analysis Thermogravimetric analysis (TGA) was employed to assess the thermal stability of Curcumin, Cas-MC, CasCur-MC, and DX-CasCur-MC (NETZSCH, Germany). The instrument was set with a heating rate of 10 °C/min under nitrogen gas rate of 50 ml min^{-1}. All measurements were conducted within a temperature range of 20–500 °C.

Curcumin release profile

To assess the amount of released curcumin in the physiological condition and the tumor microenvironment, two simulated solutions (50 ml) were individually prepared with different pH values of 7.4 and 5.5 corresponding to the two environments. Dx-CasCur-MC solution (2 ml) was poured in each cellulose dialysis bag with a molecular cutoff of 12 kDa. Subsequently, one dialysis bag was immersed in the simulated physiological solution (pH 7.4), while the other was placed in the simulated tumor microenvironment

solution (pH 5.5). Both bags were immersed in a shaker water bath maintained at 100 rpm/37 °C. At selected time points, the concentration of released curcumin was measured using a spectrofluorometer at $\lambda_{excitation} = 425$ nm and $\lambda_{emission} = 530$ nm. To assess the cumulative drug release over 48 h, the withdrawn samples were returned back to the medium after measurements. Measurements were performed in triplicate.

Radical scavenging activity

The radical scavenging activity of both unloaded curcumin and curcumin-loaded dextran-casein-methyl cellulose was assessed through the DPPH assay (Li and Chen 2022). Initially, a freshly prepared DPPH stock solution (1 ml) was mixed with 1 ml of various concentrations of the test samples (20–100 mg/ml). To prepare the control sample, ethanol (2 ml) was mixed with DPPH (1 ml). Subsequently, all mixtures were placed in a water bath shaker for 1 h in a dark environment. Post incubation time, the color change in the samples were measured using the spectrophotometer at λ_{517}. Then, the radical scavenging activity was calculated:

$$\text{Radical scavenging activity } \% = \text{Ac} - \text{As}/\text{Ac} \times 100$$

where Ac is the control absorbance and As is the sample absorbance. Measurements were performed in triplicate.

In vitro cytotoxicity

The cytotoxicity of both curcumin-loaded nanocomplex (DX-CasCur-MC) and free curcumin (Cur) on human colon cancer cells (HCT-116) was evaluated using the MTT assay. Human colorectal cancer cell line (*HCT-116*) was purchased from the American Type of Culture Collection (*ATCC*, Bethesda, MD, *USA*). In 96-well plates, the cells (5×10^3) were cultured in standard supplemented media Dulbecco's Modified Eagle Medium (DMEM) and placed for 24 h in a CO_2 incubator (5%). Then, the cells were treated individually with Cur and DX-CasCur-MC at concentrations of (0.39, 0.78, 1.5, 3.125, 6.25, 12.5, 25, 50, 100 µg/ml) and then incubated for 48 h. The cell viability percentage was measured by mixing MTT solution (10 µl) with the treated cells followed by 4 h incubation under a dark environment. Absorbance measurements were conducted at λ_{570} nm using a microplate Elisa reader (Ortenberg, Germany).

Cell cycle analysis

HCT-116 cells (10^5) were separately treated with free curcumin and curcumin loaded nanocomposite (DX-CasCur-MC) at their IC_{50} concentrations, as determined by cytotoxicity assays, over a 48-h period. Subsequently, both untreated and treated cells underwent trypsinization and were washed twice with PBS (ice-cold). Thereafter, the resuspended cells (in ice-cold ethanol solution 60%) were incubated for 1 h, at 4 °C for cell fixation. Following fixation, the cells were washed with PBS two times and ultimately resuspended in a solution of PBS, propidium iodide (10 µg/ml) and RNAase (50 µg/ml). This suspension was further incubated in dark conditions for 20 min at 37 °C. Utilizing flow cytometry, the cellular DNA content was analyzed at $\lambda_{excitation} = 535$ nm and $\lambda_{emission} = 617$ nm. The distribution of the cell cycle for cells treated with DX-CasCur-MC and curcumin was measured in comparison with the untreated ones using an instrument from ACEA-Bioscience Inc., USA. All measurement were measured in triplicate.

Autophagy

To quantify the autophagic cell death induced in colorectal cancer cells (HCT-116) upon treatment with curcumin and DX-CasCur-MC, flow cytometry analysis was utilized employing acridine orange stain. HCT-116 cells (10^5) were treated with curcumin and DX-CasCur-MC for 48 h at their IC_{50} concentrations. Both untreated and treated cells were trypsinized, washed with ice-cold PBS, stained with acridine orange, and incubated for 30 min at 37 °C in a dark environment. Following staining, all cells were analyzed using the ACEA NovocyteTM flow cytometer, and the emitted fluorescence signals of acridine orange were captured by the signal detector at $\lambda_{excitation} = 488$ nm and $\lambda_{emission} = 530$ nm. The data were quantified as net fluorescence intensity (NFI) using NovoExpress software (ACEA-Bioscience Inc., USA) (Abdel-Sattar et al. 2023).

Comet assay

The Comet assay, or single-cell gel electrophoresis was employed to quantify the extent of DNA damage in HCT-116 cells following treatment with curcumin and DX-CasCur-MC. HCT-116 cells (10^5) were cultured in a 12-well plate and treated separately with curcumin and DX-CasCur-MC for 48 h. Aliquots from both untreated and treated cells were collected and applied to microscopic slides, following the procedure outlined in a previous study (Lin et al. 2007). Subsequently, in situ DNA lysis in the nucleus was performed. All cells were subjected to gel electrophoresis, and the visualized DNA was stained with ethidium bromide (EB) and captured using a fluorescence microscope. The observed comet structures, indicative of DNA damage in treated cells, were quantified in terms of comet tail lengths and other parameters using CometScore™ software.

In vitro digestion experiment

Since the study aimed to develop an oral drug delivery system, the behavior of DX-CasCur-MC in gastrointestinal fluids, in terms of hydrodynamic size distribution and curcumin release, was evaluated following a previously established protocol with minor modifications (Xu et al. 2020). In brief, simulated gastric fluid (SGF) was prepared by combining pepsin (3.2 mg/ml) and NaCl (2 mg/ml) formulating a simulated gastric digestion environment (pH 2). To prepare simulated intestinal fluid (SIF), pancreatin (3 mg/ml) was mixed with NaCl (8.8 mg/ml) at pH 7. The experimental procedure commenced by mixing a DX-CasCur-MC solution (2 ml) with SGF, and then incubating for 1 h in a shaker-water bath (100 rpm at 37 °C). In another tube, SIF (pH = 7) was mixed with DX-CasCur-MC and then incubated for 2 h in a shaker-water bath (100 rpm at 37 °C). Hydrodynamic size distribution of the digestion was measured at specified time points (1 h post incubation in SGF and 2 h post incubation in SIF). The quantity of the released curcumin from the nanocomposite was measured spectrofluorometrically and calculated using a calibration curve (Chen et al. 2020).

In vivo study

Animals In this study, 15 female Balb/c mice, weighing 20–25 g and aged 4–5 weeks (purchased from the animal house of the National Cancer Institute, Cairo, Egypt) were used. The mice were housed in standardized cages with continuous access to water and food, controlled air humidity, and a 12-h dark/light cycle for the duration of the experiment. Ehrlich ascites tumor (EAT) cells (1×10^6) was inoculated into the right flank of the mice and monitored until the formation of a subcutaneous solid tumor reached a size of 0.5 cm^3(Elbialy and Mohamed 2020). Tumor bearing mice were divided into 3 groups, with 5 mice in each group: a control group, a curcumin treated group, and a DX-CasCur-MC treated group.

Ethics The experiment received approval from Cairo University's Institutional Animal Care and Use Committee (CU-IACUC) (Egypt) under the reference CU-I-F-71-22. All experimental procedures adhered to CU-IACUC standards, following guidelines from the Council for International Organization of Medical Sciences and the International Council for Laboratory Animal Science (CIOMS/ICLAS, 2012), as well as the American Guide of Animal Care and Use. The study was reported in accordance with ARRIVE guidelines.

Tumor growth inhibition assessment To investigate the growth inhibitory effect of DX-CasCur-MC compared to free curcumin and untreated mice, animals were randomly divided into three groups. Group 1 (control) received 100 µl saline orally, Group 2 received 100 µl curcumin solution (4 mg/kg) orally, and Group 3 received 100 µl of DX-CasCur-MC (4 mg/kg) nanoparticle solution orally. They were administered 5 doses/ 15 d.

Throughout the two-week experiment, tumor volume was measured every three days using an electronic caliper. At the time of experiment termination, the body weight of all groups was recorded. Subsequently, mice from each group were weighted, euthanized, and the tumors were collected and weighed. Tumors from each group were preserved in a 10% formalin solution for histopathological examination. Tumors were embedded in paraffin, sectioned, and stained using hematoxylin and eosin (H&E).

Statistical analysis Data were presented as mean ± standard deviation (SD). Multiple comparison was performed using ANOVA analysis (SPSS, software 29.0), with p value < 0.05 considered as significant difference (*).

Results and discussion

Synthesis of dextran-casein-methyl cellulose encapsulated curcumin

Numerous studies have highlighted the exceptional capability of casein nanoparticles in encapsulating and delivering bioactive compounds (nutraceuticals) to specific diseased sites. However, a notable challenge arises as the encapsulated drug tends to leak outside casein micelles when exposed to human body temperature (~ 37 °C) and physiological fluids (Xv et al. 2020). Consequently, optimizing casein micelles through conjugation with a supportive material, such as polysaccharides, becomes imperative. Leveraging its emulsifying property, casein can be effectively combined with polysaccharides to form a nanocomplex that harnesses the advantageous properties of both components.

This issue is addressed by encapsulating curcumin within casein micelles, followed by conjugation with methylcellulose and coating with dextran. Curcumin was encapsulated within casein nanomicelles via the property of self-assembling to form CasCur which stabilized by the addition of methyl cellulose (CasCur-MC). The nanocarrier stabilization was further enhanced by dextran coating (DX-CasCur-MC). It should be mentioned that the hydrophobic interaction between casein and curcumin would promote curcumin stability with high encapsulation efficiency. Additionally, the hydrogen bonding and electrostatic interaction between the protein and polysaccharides provides the nanocarrier the appropriate response in different physiological media. The preparation method has the advantage of being simple with the production of high yield. The encapsulation efficiency of curcumin within the proposed nanocomplex system was 92%.

Characterization of the synthesized nanocomplex (DX-CasCur-MC)

Transmission electron microscopy

The morphological structure of the nanoparticles was revealed using TEM both before and after loading curcumin. TEM images illustrated the size and morphology of Cas-MC and DX-CasCur-MC (Fig. 1a, b). The fabricated nanoparticles exhibited a spherical shape with a size exceeding 200 nm (Fig. 1a). Following curcumin loading, DX-CasCur-MC exhibited a darker appearance with a distinct coating layer enveloping the nanoformulation (Fig. 1b).

Hydrodynamic size distribution and zeta potential measurements

The hydrodynamic diameters of Cas-MC and DX-CasCur-MC are presented in Fig. 1c. The unloaded sample exhibits an average diameter of 295 ± 32 nm, whereas the curcumin-loaded sample demonstrates a reduced average hydrodynamic diameter of 220 ± 42 nm. This size reduction in the nanocomplex (DX-CasCur-MC) upon curcumin encapsulation can be attributed to the contraction of the internal protein nanostructure as curcumin fills the inner cavities of casein micelles. This phenomenon arises from the combined effects of hydrogen bonding, as well as both hydrophobic and electrostatic interactions between curcumin and the active groups of casein. These findings align with a prior study (Li and Chen 2022). Fortunately, the developed micelle diameter is suitable for drug delivery purposes, allowing it to evade renal clearance (Gaucher et al. 2005).

Measuring zeta potential at each stage of preparation acts as a predictive tool for assessing the colloidal stability of the nanocarriers and the effectiveness of the preparation method. The measured zeta potential values for Cas-MC, CasCur-MC, and DX-CasCur-MC are −10.8 ± 1.68, −8.99 ± 1.25, and −6.56 ± 0.97 mV, respectively (Fig. 1d). These values reflect the impact of curcumin loading and dextran coating steps in reducing the negativity of the nanoconjugate. The decrease in the negative charge of DX-CasCur-MC can be attributed to the coating effect of the formed dextran layer on the nanoparticle surface. Zeta potential values offer insights into the stability

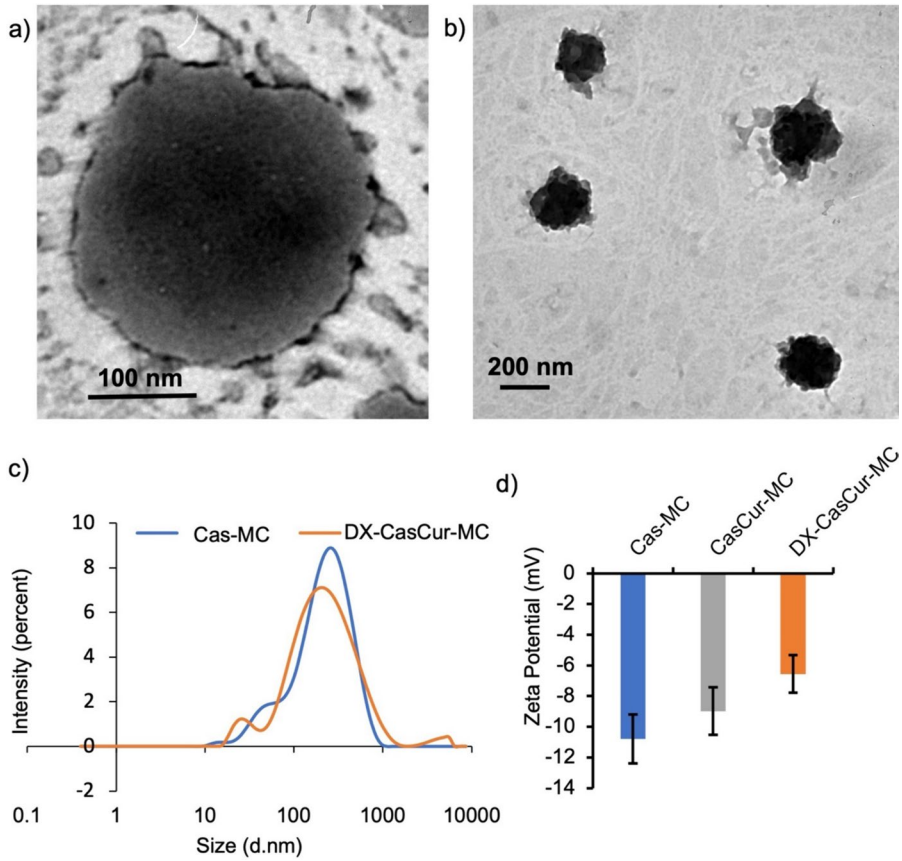

Fig. 1 Characterization of DX-CasCur-MC: transmission electron microscopic images for **a** Cas-MC, **b** DX-CasCur-MC, **c** size distribution measurements of curcumin loaded (DX-CasCur-MC) and unloaded uncoated nanoconjugate (Cas-MC), **d** zeta potential values of Cas-MC, CasCur-MC and DX-CasCur-MC, measurements for were performed in triplicate and represented as mean and ± SD

and the behavior of the developed nanocomplex in biological systems (Jin et al. 2019).

Fluorescence spectroscopy

Protein intrinsic fluorescence arises from tryptophan residues located in the hydrophobic cavities within protein tertiary structure. The fluorescence spectra of Cas-MC, CasCur-MC, and DX-CasCur-MC were measured to elucidate the interaction between curcumin and the Cas-MC nanocarrier, as well as the conformational changes in the protein upon dextran coating (Fig. 2a, b). The nanocarrier composed of Casein-methylcellulose (Cas-MC) exhibited a strong fluorescence emission peak at $\lambda_{emission} = 341$ nm, representing the tryptophan and tyrosine residues in the protein. Following curcumin encapsulation, both protein fluorescence emission peaks exhibited a slight blue shift to 339 nm, accompanied by a slight decrease in intensity, indicating alterations in the curcumin microenvironment due to the interaction with casein residues through hydrophobic interaction (Xu et al. 2017).

As illustrated in Fig. 2a, b, the conjugation of Cas-MC with dextran significantly reduced the maximum fluorescence peak to ~ 65%. This substantial reduction in fluorescence intensity suggested the successful conjugation of CasCur-MC with dextran, leading to the formation of a dextran shell around CasCur-MC micelles. Importantly, the maximum fluorescence peak position shifted to 332 nm (blue shift), indicating that the conjugation between CasCur-MC and dextran protected the CasCur-MC nanocarrier from denaturation or conformational changes. The observed blue shift also suggested the burial of tryptophan residues into the hydrophobic microdomains of DX-CasCur-MC micelles (Liu and Guo 2008). Previous studies have reported that a red shift in the fluorescence peak after protein-polysaccharide conjugation is indicative of protein unfolding and denaturation (Wu and Wang 2017). The modified preparation method developed in this study has the advantage of

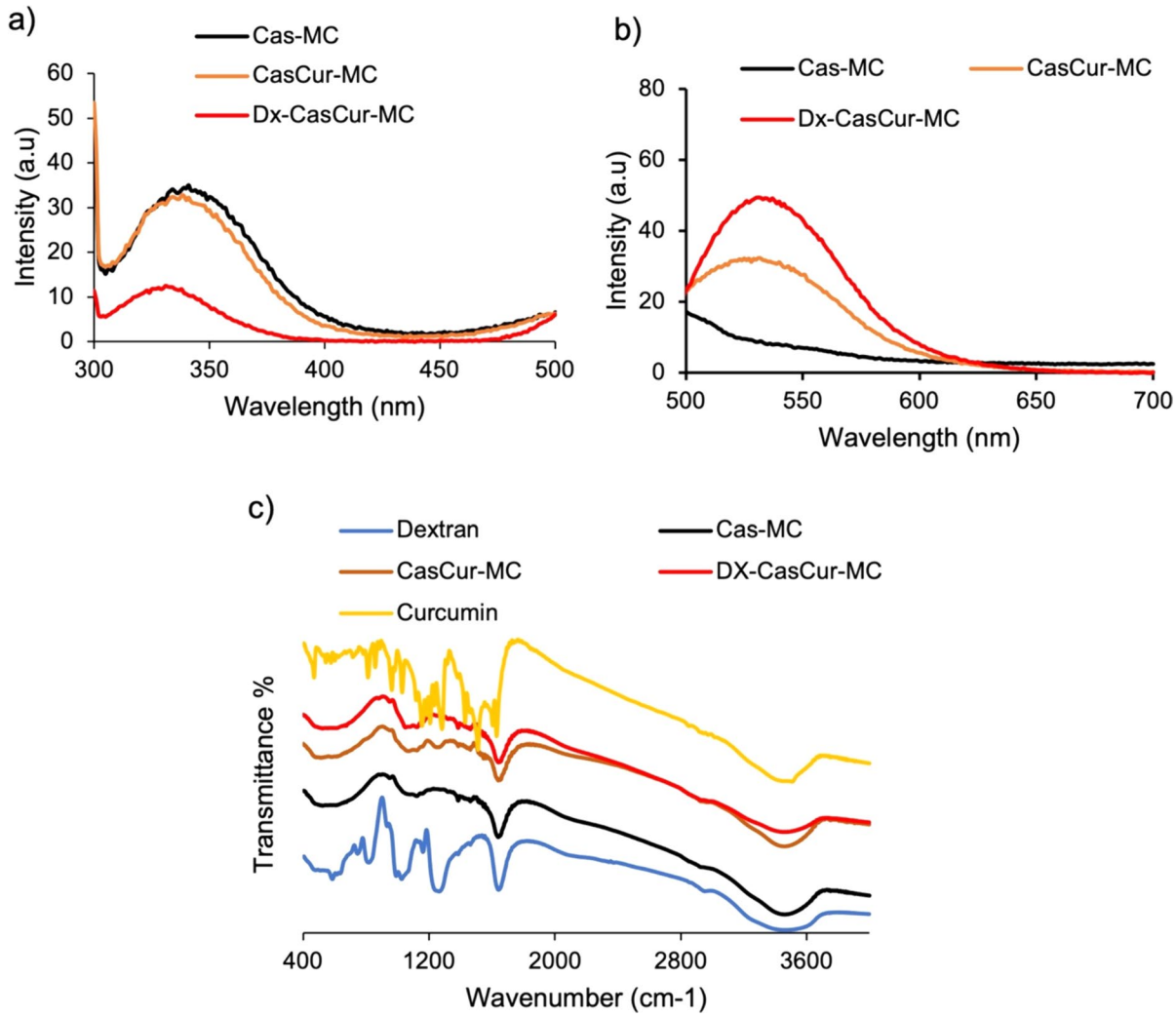

Fig. 2 Fluorescence and FTIR spectroscopy: fluorescence emission spectra of Cas-MC, CasCur-MC, and DX-CasCur-MC: **a** at protein excitation wavelength 280 nm, **b** at curcumin excitation wavelength 425 nm. **c** FTIR spectra of: dextran, curcumin, Cas-MC, CasCur-MC, DX-CasCur-MC

preventing protein denaturation, as confirmed by the observed blue shift in the fluorescence peak.

The intrinsic fluorescence of curcumin is commonly employed to investigate the binding between proteins and curcumin. This conjugation exhibited a sensitive response reflected in the position and intensity of its fluorescence peak. Literature documents indicate that the fluorescence peak of free curcumin appears with low intensity at ~ 550 nm, indicating instability and fluorescence quenching in a polar environment (Began et al. 1999; Khadem Sadigh et al. 2017). The conjugation of curcumin with casein and methyl cellulose shifted the curcumin peak to 335 nm (blue shift) (see Fig. 2b). The fluorescence spectrum of DX-CasCur-MC showed a further blue shift in the curcumin fluorescence peak (330 nm) accompanied by higher intensity upon conjugation with dextran. Conjugation with protein and polysaccharides induced a blue shift in the curcumin emission peak with an enhancement in fluorescence intensity, demonstrating a change in curcumin structure induced by its interaction with the matrices. This change is attributed to the transfer of curcumin from a hydrophilic environment to the hydrophobic region of casein

and dextran micelles (Wu and Wang 2017). Consequently, curcumin fluorescence quenching is reduced, and fluorophore stability is increased, leading to an enhancement in fluorescence intensity (Li and Wang 2015).

Fourier-transform infrared spectroscopy

The protein-polysaccharide conjugation was verified through FTIR analysis, which illustrated distinctive structural bands associated with the functional groups of each component before and after the conjugation process (Fig. 2c). The FTIR spectrum of Cas-MC indicated the emergence of primary characteristic bands from both methyl cellulose and casein, accompanied by observable shifts. Notably, the FTIR absorption peaks of casein, including amide I, amide II, and O–H stretching, exhibited a shift from 1514, 1637, and 3281 to 1461, 1639, and 3477 cm^{-1}, respectively, upon conjugation with methyl cellulose. Similarly, the principal characteristic bands of methyl cellulose at 1460, 1380, and 950 cm^{-1} (as per literature) experienced shifts upon conjugation with casein (Oliveira et al. 2015).

The conjugation between casein micelle and methyl cellulose can be attributed to their interaction through hydrogen bonds involving functional groups such as amino groups, carboxyl groups, and amide bonds. This interaction resulted in noticeable alterations in the absorption bands within the FTIR spectrum.

The FTIR spectrum of dextran unveiled its characteristic bands at 1160, 1022, and 916 cm^{-1}. The absorption band at 1160 cm^{-1} is associated with C–O–C vibrations and glycoside linkage, while the band at 1022 cm^{-1} signifies the flexibility of the dextran chain in relation to glycosidic bonds. The observed band at 916 cm^{-1} is attributed to $\propto$-D-glucan (Shukla et al. 2011). Peaks corresponding to dextran displayed shifts in the DX-CasCur-MC spectrum, indicating the successful conjugation with CasCur-MC.

The characteristic absorption bands of curcumin appeared at 3510 cm^{-1} and 1628 cm^{-1}, corresponding to phenolic O–H stretching and C=C/C=O stretching, respectively. Additionally, bands at 710 and 870 cm^{-1} were observed, corresponding to different C–H motions (Bich et al. 2009). The analysis of the FTIR spectrum of the final formulation, Dx-CasCur-MC, demonstrated the presence of all characteristic bands from each constituent, accompanied by shifts indicative of successful conjugation.

X-ray diffraction analysis

The crystalline diffraction patterns of Cas-MC, CasCur-MC, Cur, and DX-CasCur-MC were examined. It is well-documented in the literature that casein exhibits an amorphous structure, while methyl cellulose (MC) is semicrystalline, with diffraction peaks appearing at 8.5° and 20.6° (Oliveira et al. 2015; Xu et al. 2020). The conjugation of MC with casein resulted in a shift in the diffraction peaks of MC, as illustrated in the Cas-MC XRD spectrum (Fig. 3a).

The amorphous nature of dextran is indicated by a diffraction peak at 21.7°, as reported in a previous study (Yuan et al. 2020). The dextran peak underwent a shift upon interaction with CasCur-MC, forming the final nanocomplex (DX-CasCur-MC), as illustrated in Fig. 3a. To assess the ability of the proposed nanocarrier to encapsulate curcumin and address challenges related to its poor solubility, the XRD pattern of DX-CasCur-MC was investigated.

Considering the information available, curcumin typically exhibits multiple peaks in its XRD pattern due to its crystallinity, this is then coupled with the semicrystallinity of MC and the amorphous nature of both casein and dextran (Li et al. 2022a). Consequently, the conjugation of curcumin with the protein–polysaccharides nanocomplex resulted in a reduction of curcumin crystallinity. This reduction, in turn, enhances curcumin's solubility, bioavailability, and ultimately its biological activity (Benzaria et al. 2013). Despite the amorphous nature of casein, the presence of the minor crystalline peaks in CasCur-MC and DX-CasCur-MC can be attributed to the possibility that a fraction of the encapsulated curcumin protruded from Cas-MC micelles.

Thermogravimetric analysis

The TGA thermograms of Curcumin (Cur), Casein-methylcellulose (Cas-MC), CasCur-MC, and Dextran-coated CasCur-MC (DX-CasCur-MC) are presented in Fig. 3b. Initially, the observed weight loss in the temperature range of 20–150 °C is minimal and is attributed to the desorption or dehydration of water from the polysaccharides. This is followed by

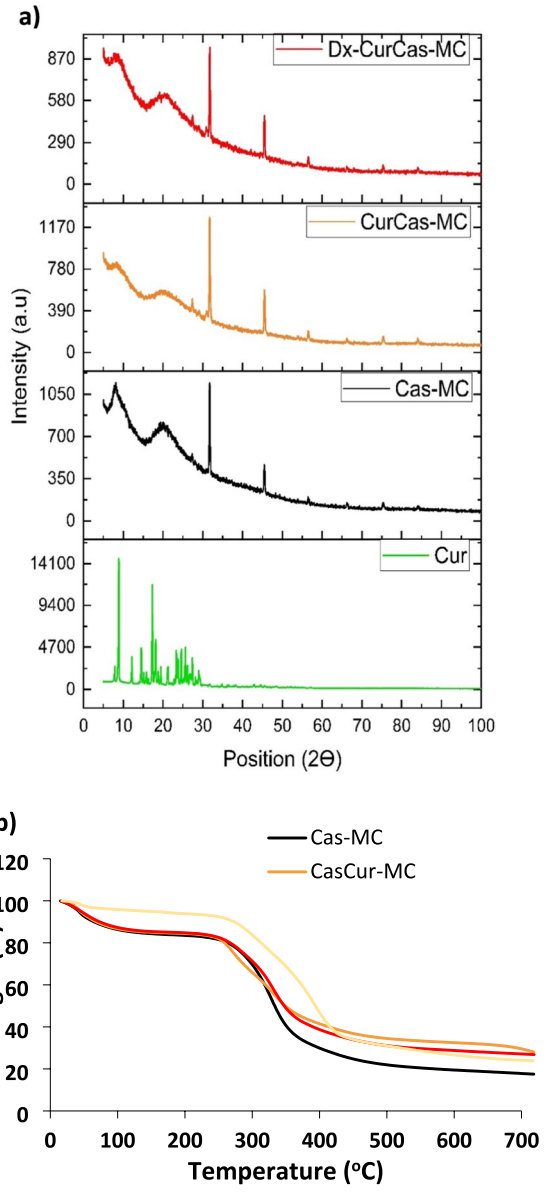

Fig. 3 X-ray diffraction and thermogravimetric analysis: **a** XRD patterns of: Cur, Cas-MC, CasCur-MC and DX-CasCur-MC. **b** TGA thermograms for Cur, Cas-MC, CasCur-MC, and DX-CasCur-MC

pyrolytic decomposition and depolymerization in the range of 160–258 °C. Subsequently, above 350 °C, the samples undergo decomposition, resulting in the release of CO, CH4, and water (Oliveira et al. 2015). In the TGA scan for CasCur-MC, an initial weight loss of approximately 16% occurred at 134 °C. Both Cas-MC and DX-CasCur-MC exhibited an initial weight loss of about 18% at 147.7 °C. Both Cas-MC and DX-CasCur-MC displayed a rapid thermal decomposition rate at 175 °C, reaching total weight losses of 76.6% and 83% at 450 °C, respectively. In the case of CasCur-MC, a rapid thermal decomposition rate was observed at 150 °C, resulting in a 73% weight loss at 421 °C. Due to its hydrophobic nature, the thermal behavior of curcumin is notably different. Uponreaching 140 °C, there was no significant weight loss, followed by rapid thermal decomposition at 173.5 °C, ultimately reaching a 77% weight loss at 450 °C.

In vitro study

Curcumin release profile

Designing an effective drug delivery system requires a thorough investigation into the behavior of the released drug from the nanocarrier. Consequently, we studied the release of curcumin from the nanocomplex DX-CasCur-MC in two distinct environments: physiological (pH 7.4) and tumor (pH 5.5). Figure 4a illustrates the cumulative release percentage of curcumin at both tested pH levels over 48 h.

The release profile exhibited a steady-state pattern in both acidic and physiological pH conditions, with no observable burst effect. Notably, drug release in the acidic environment demonstrated an approximately twofold increase compared to the physiological environment at each time point. Sustained release commenced at 16 h and reached its peak at 68% at pH 5.5 and 57% at pH 7.4 after 48 h. Additionally, the results revealed that approximately 30% of the drug remained within the nanocomplex after 48 h.

The incorporation of methylcellulose and dextran coating with casein nanoparticles optimized the performance of the hybrid nanoparticles, resulting in controlled and sustained release of curcumin in both physiological and acidic media. The observed cumulative release percentages of curcumin in both media were attributed to the drug concentration gradient between the fluid layer surrounding the nanocarrier's surface and the release media. Importantly, the obtained release behavior indicated no discernible degradation in the integrity of the bio-nanocomposite or surface deformation (Chen and Subirade 2005; Keshavarz et al. 2023). Consequently, the conjugation facilitated the bio-nanocomplex carrier in achieving a

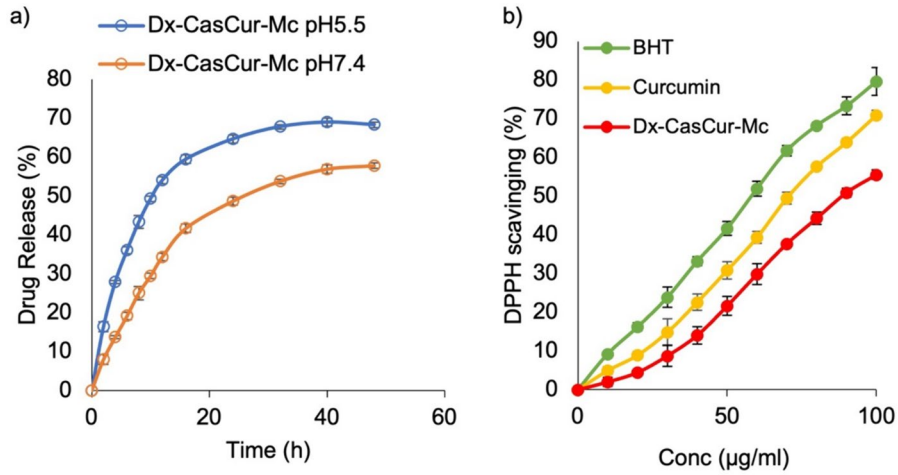

Fig. 4 Curcumin release profile and antioxidant activity: **a** cumulative curcumin release profile at pH 5.5 and pH7.4. **b** DPPH radical scavenging activity of Curcumin, DX-CasCur-MC, and the standard BHT. All measurements were performed in triplicate and represented as mean and ± SD

superior sustained drug release compared to carriers composed of protein or polymeric nanoparticles alone (Luo et al. 2011).

Upon reviewing the literature, a similar study by Chen, Y. et al. (2024), fabricated a curcumin nanocarrier by conjugating soy protein with two polysaccharides. This nanoconjugation achieved high drug encapsulation efficiency (95%) with improved anticancer activity (Chen et al. 2024). In contrast, the conjugation of zein protein with a single polysaccharide (either hyaluronic acid or pectin) demonstrated instability in simulated gastrointestinal fluids (44% and 26% respectively) (Liu et al. 2022c). Similarly, the conjugation of zein protein with chitosan as a nanodelivery system for curcumin and berberine showed low drug encapsulation efficiency (75%) and drug release 39% and 71% at pH 7.4 and 5.5 respectively (Ghobadi-Oghaz et al. 2022).

Antioxidant activity

The antioxidant scavenging capacity of both curcumin and the curcumin-loaded nanocomplex was assessed through the DPPH assay. As depicted in Fig. 4b, the scavenging activity of curcumin against DPPH free radicals appeared to be higher than that of DX-CasCur-MC, although the increase was not statistically significant. This difference is attributed to the dissolution of curcumin in ethanol and the direct contact between curcumin and DPPH free radicals during the incubation period. On the contrary, the nanocomplex exhibited a restricted release of curcumin during the 30-min incubation period, leading to a diminished radical scavenging capability. This behavior can be elucidated by examining the curcumin release profile from the nanocomplex at pH 7.4, revealing that the released curcumin did not surpass 8% within a 2 h timeframe, (see Fig. 4a). At the highest concentration (100 µg ml^{-1}), the measured radicals scavenging capability of DX-CasCur-MC was 55.5%, whereas curcumin exhibited a higher scavenging capability reached 71% at the same concentration.

Cytotoxicity

Figure 5a–c illustrate the morphological changes in HCT-116 cancer cells upon exposure to DX-CasCur-MC and curcumin, as compared to untreated cells, using an inverted optical microscope. The concentration-dependent cytotoxic activity of both curcumin and DX-CasCur-MC against the HCT-116 cell line is presented in Fig. 5d. The maximum cytotoxic effects induced by DX-CasCur-MC and curcumin were 58% and 50%, respectively. The calculated IC_{50} values were 26.9 µg/ml for DX-CasCur-MC and 45.2 µg/ml for curcumin. The results demonstrated that lower dose of encapsulated curcumin is quite enough to induced higher cytotoxic effect against cancer cells than free curcumin. Thus, indicating the ability of the nanocarrier to enhance curcumin solubility and bioavailability in comparison with free curcumin. This attributed to the synergistic effect of protein–polysaccharides nanocomplex. Therefore, the present study lays the groundwork for the development of a novel treatment approach where curcumin, combined with

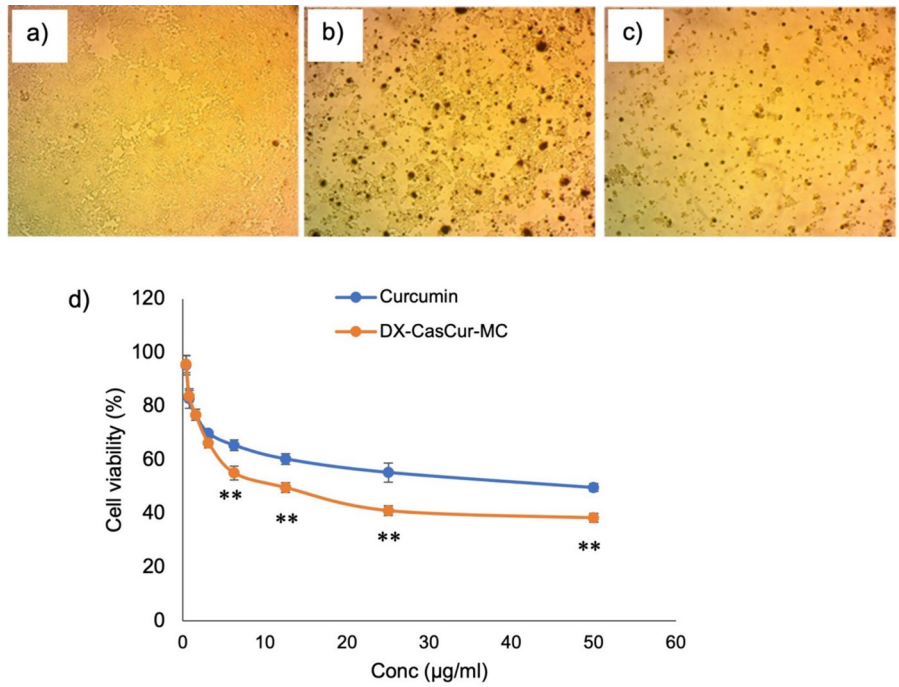

Fig. 5 Morphology of **a** control cells, **b** curcumin treated cells, and **c** DX-CasCur-MC treated cells. **d** Cell viability percent of HCT-116 cancer cells upon exposure to different concentrations of DX-CasCur-MC and curcumin post 48 h incubation time, measurements were performed in triplicate and represented as mean and ± SD

casein and two polysaccharides, effectively induces cytotoxic effects on HCT-116 cancer cells.

Cell cycle analysis

A comprehensive understanding of the effectiveness of the proposed therapeutic agent (DX-CasCur-MC) against HCT-116 cancer cells can be obtained through a detailed analysis of the cell cycle. The distribution of the cell cycle was examined to further investigate the antiproliferative activity of encapsulated curcumin (DX-CasCur-MC) compared to free curcumin against HCT-116 cells. Utilizing a flow cytometric assay, we investigated the impact of both DX-CasCur-MC and curcumin on the distribution of cell cycle phases in HCT-116 cells (refer to Fig. 6a). Exposure to curcumin (45.2 µg ml^{-1}) for 48 h resulted in a significant increase in the cell population in both sub G1 (from 4.14% ± 0.328 to 8.19% ± 1.42, $p \leq 0.008$) and S phase (from 8.84% ± 1.09 to 14.86% ± 1.38, $p \leq 0.0041$) compared to untreated cells, indicating cell cycle arrest in these two phases. Conversely, curcumin led to a non-significant reduction in the cell population in G1 (from 65% ± 1.122 to 52.77% ± 3.52) and G2/M (from 30.88% ± 1.93 to 27.56% ± 0.84) relative to untreated cells (Left column of Fig. 6a).

In comparison to untreated cells, DX-CasCur-MC induced a sharp increase in the cell population in the sub G1 phase, from 4.14% ± 0.328 to 28.64% ± 0.76, $p < 0.0001$) indicating apoptosis induction and cell cycle arrest. Reciprocally, DX-CasCur-MC led to a substantial decrease in G1 (from 65% ± 1.122 to 28.77% ± 1.81, $p < 0.0001$), S (from 8.84% ± 1.09 to 7.5% ± 0.355), and G2/M (from 30.88% ± 1.93 to 27.12% ± 0.84). Previous studies have shown that cell cycle arrest in the sub G1 phase is attributed to functional disruption in cyclin-dependent kinases (Blume-Jensen and Hunter 2001; Noble et al. 2004).

Figure 6b illustrates the cell cycle profile for control HCT-116 cells, where the major cell population appears in G1 (65% ± 1.122), S phase (8% ± 1.09), and (30.88% ± 1.93) proliferative cells at G2/M. Meanwhile, the measured dead cells at sub G1 were 4.14% ± 0.328. Treating HCT-116 cells with DX-CasCur-MC prompted a significant increase in the population of dead cells, reaching 28.64%, compared to 4.14% for untreated cells (control) and 8.19% for curcumin-treated cells, suggesting a notable cell cycle arrest for loaded curcumin. These results align with a previous study (Sala de Oyanguren et al. 2020).

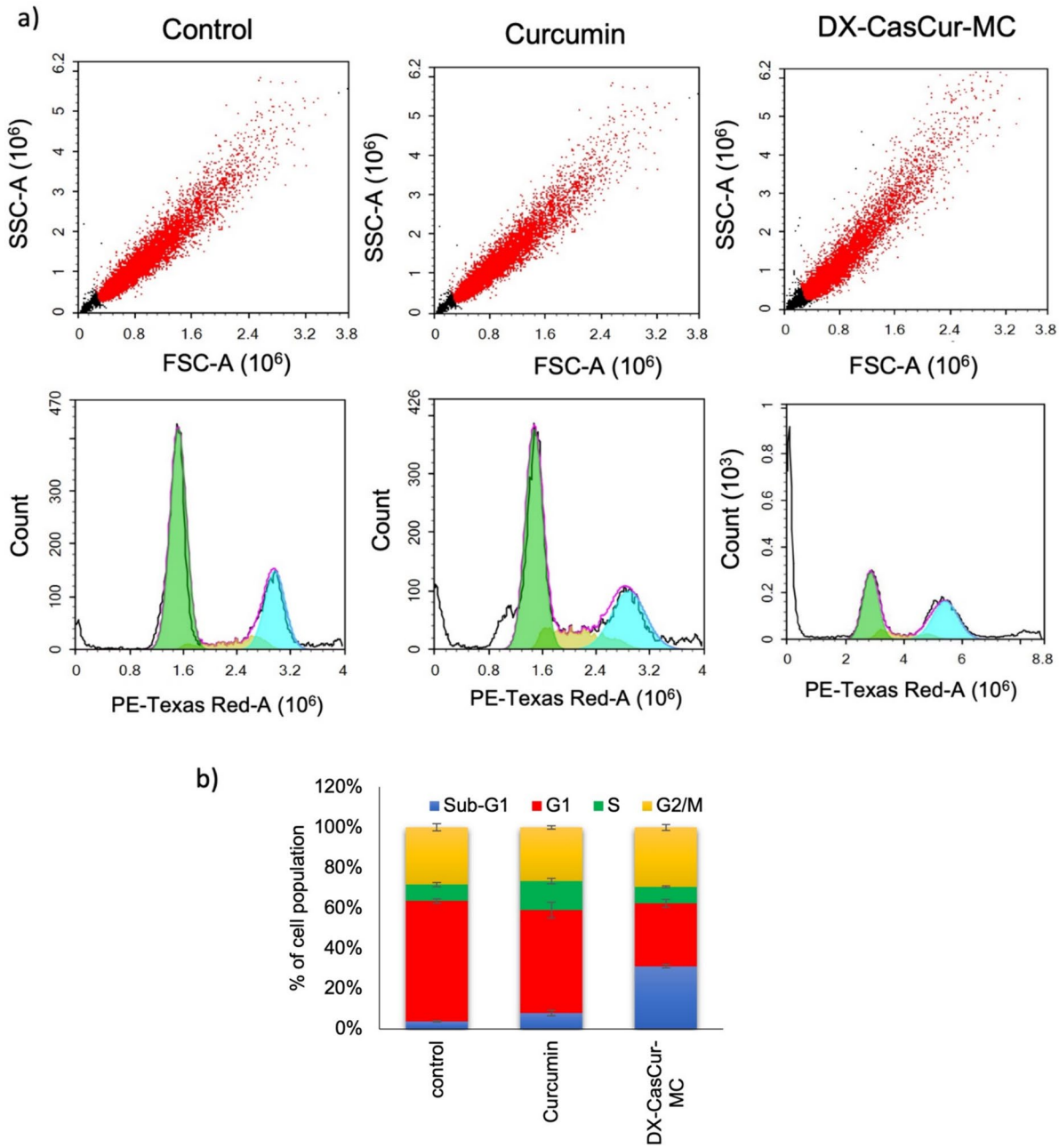

Fig. 6 Flow cytometric analysis: **a** cell cycle distribution of HCT-116 cells post exposure to curcumin and DX-CasCur-MC for 48 h, **b** plot of different cell cycle phases as a percentage of total events. Data is represented as mean ± SD (n = 3), the statistical significance difference in comparison with untreated cells is (*) ($p < 0.05$), (**) ($p < 0.01$), (***) ($p < 0.001$)

Autophagy

In addition to assessing cytotoxicity and cell cycle distribution, we conducted further investigations to explore the impact of DX-CasCur-MC compared to free curcumin on colorectal cancer cells, specifically focusing on the autophagy process. Recent studies have highlighted the involvement of autophagy in the anticancer activity of curcumin. Therefore, we aimed to determine whether the induction of cancer cell

death by both free curcumin and the curcumin-loaded nanocomposite (DX-CasCur-MC) is associated with autophagy as one of the mechanisms of cancer cell death.

Colorectal cancer cells (HCT-116) were treated separately with curcumin and DX-CasCur-MC for 48 h. Subsequently, we used acridine orange and flow cytometry to assess autophagy induction in cells treated with curcumin and DX-CasCur-MC, comparing the results with untreated cells (refer to Fig. 7a, d). The analysis revealed that HCT-116 cells treated with free curcumin exhibited a 24% increase in autophagic signals relative to the control group (Fig. 7b, d). Interestingly, cells treated with the curcumin-loaded nanocarrier (DX-CasCur-MC) showed a significant enhancement in autophagic signals, with a 51.5% increase compared to untreated cells (Fig. 7c, d). These results affirm the nanocomplex's role in enhancing curcumin's efficacy against cancer cells by inducing autophagy process.

The observed autophagic results align with previous studies that have explored the role of curcumin in inducing autophagy, ultimately contributing to the

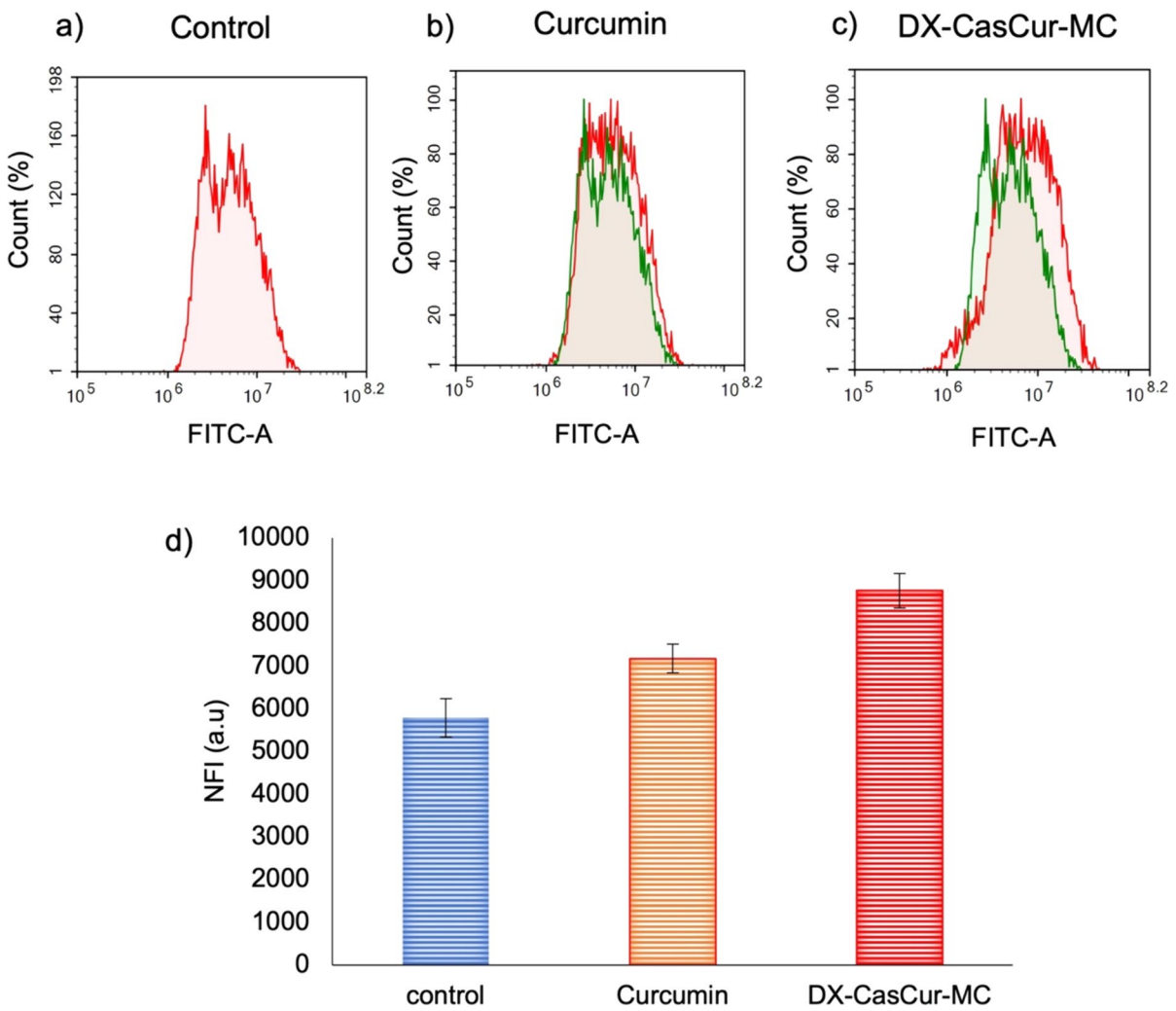

Fig. 7 Autophagy: **a–c** Assessment of cell death induction by autophagy in colorectal cancer cells (HCT-116) post treatment with DX-CasCur-MC and curcumin relative to untreated cells. **d** Net fluorescence intensity (NFI) for untreated, and both DX-CasCur-MC and curcumin treated colorectal cells. Data is presented as mean ± SD (n = 3) and the statistical significance with control is presented by (*) ($p < 0.05$) and (**) ($p < 0.01$)

suppression of cancer cell proliferation (Xiao et al. 2013; Guan et al. 2016).

The integrated results of cytotoxicity, cell cycle analysis, and autophagy clearly demonstrate the crucial role of DX-CasCur-MC in overcoming the obstacles associated with utilizing curcumin. Curcumin, in its solid form, suffers from low water solubility, which hinders its uptake, and rapid degradation in alkaline environments. A successful strategy to overcome these challenges involves incorporating curcumin into a specifically designed nanocarrier. Encapsulation of curcumin in a protein-polysaccharide nanocarrier enhances its solubility and enables it to disrupt cancerous cell metabolism. This leads to the induction of mitochondrial apoptosis through the activation and release of cytochrome c and the caspase family, culminating in the production of reactive oxygen species (ROS). These ROS then activate numerous signaling pathways that potentiate cell cycle arrest. Such cellular mechanisms significantly reduce the viability of HCT-116 cells, as observed in MTT assays (Beltzig et al. 2021). The induction of cancer cell apoptosis is also evident in inverted microscopic images. Additionally, transforming curcumin into an amorphous form allows it to target multiple molecular pathways in cancer cells, such as p53, EGFR, and NF-kB (Shehzad et al. 2010; Bortel et al. 2015; Kasi et al. 2016).

Furthermore, overcoming the challenge of curcumin solubility through its conjugation with DX-Cas-MC facilitates the activation of curcumin's molecular mechanisms targeting apoptosis and autophagy in cancer cells. Apoptosis, or programmed cell death, is associated with the activation of the caspase family, which induces cancer cell death (Ashrafizadeh et al. 2020). In contrast, autophagy involves a different molecular pathway, encompassing the degradation of cellular macromolecules and organelles via lysosomes. Lysosomal biomarkers and autophagy-related proteins (ATG) are key indicators of autophagy (Xie 2021).

Comet assay

Further research has been undertaken to assess the crucial role of the proposed nanocomplex in amplifying curcumin's effectiveness in promoting cancer cell damage. The Comet assay, a highly valuable tool for quantifying DNA damage in cancerous cells, was employed to compare the effects of encapsulated curcumin with its free form. The Comet image of HCT-116 cells treated with DX-CasCur-MC revealed substantial DNA damage compared to cells treated with free curcumin or those left untreated, as depicted in Fig. 8a–c. All Comet assay parameters, including % DNA damage, % of DNA in the tail, tail moment, and olive tail moment, corroborated the significant DNA damage in HCT-116 cells induced by DX-CasCur-MC in comparison to free curcumin, as illustrated in Fig. 8d–g.

The nanocomplex, consisting of dextran, casein, and methyl cellulose, efficiently facilitated the cellular uptake and solubility of curcumin. This facilitation enabled the induction of extensive DNA damage, ultimately leading to the demise of cancer cells. Recent studies have highlighted that curcumin's potential to inhibit cancer growth is not solely attributed to apoptosis induction but also involves destabilizing the endoplasmic reticulum and promoting autophagy (Sala de Oyanguren et al. 2020). Consequently, the enhanced therapeutic efficacy of curcumin achieved through the protein-polysaccharide nanocarrier positively impacts curcumin's role in amplifying cancer cell death.

The above integrated in vitro results provided strong evidence that we have proposed a promising category made of naturally occurring materials demonstrating enhanced physicochemical properties and anticancer activity. The behavior of the nanocomplex in physiological media and enzymes allowed its classification within oral drug delivery systems and encouraged us to move to the in vivo study.

In vitro release in simulated fluids

The oral delivery of curcumin through DX-CasCur-MC necessitates an examination of the sequential digestion impact of gastric and intestinal fluids on the nano-vehicle. Assessing the suitability of the proposed nanocomplex (DX-CasCur-MC) for oral curcumin delivery involves investigating its sequential digestion in simulated gastric and intestinal fluids. Therefore, we studied the ability of DX-CasCur-MC to withstand the challenge posed by gastric and intestinal digestive enzymes, analyzing changes in the nanoparticles' size and cumulative percentage of released curcumin. The alterations in DX-CasCur-MC size and curcumin release during incubation in

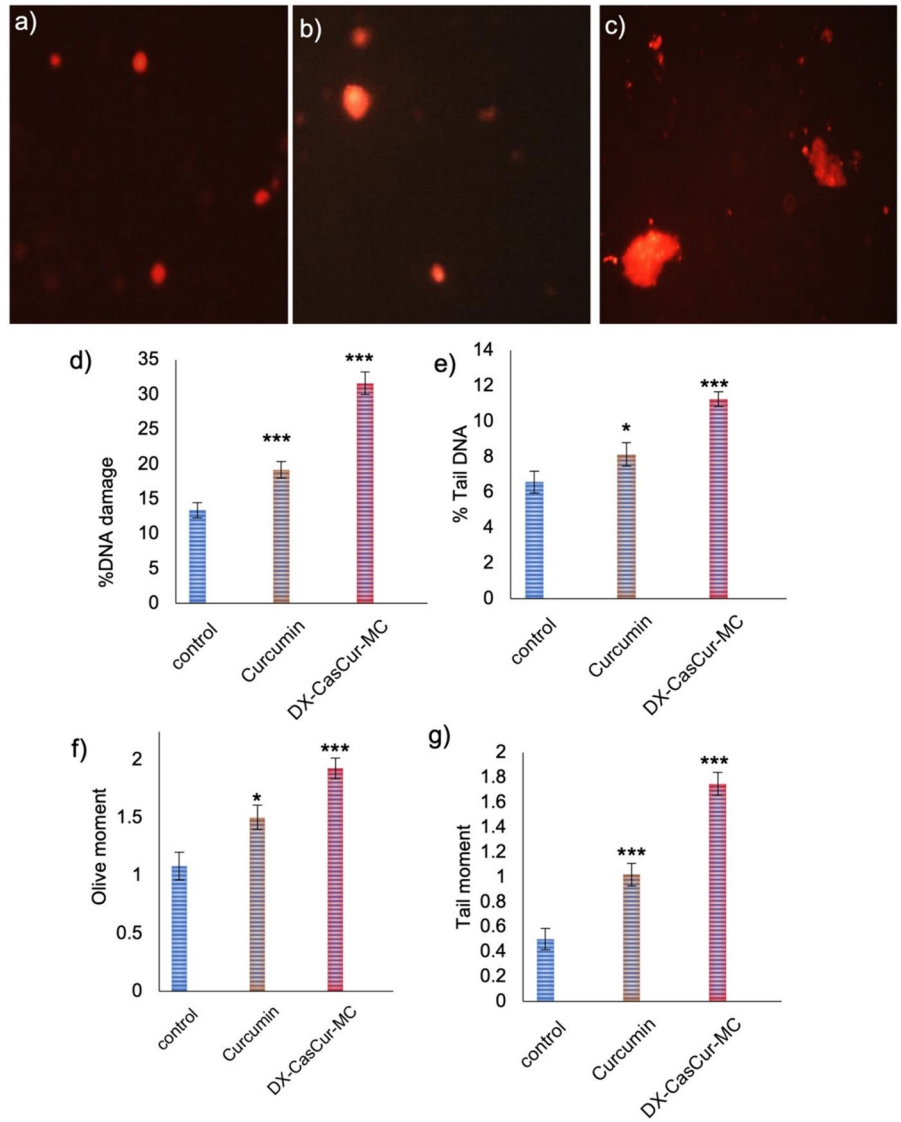

Fig. 8 Comet images of HCT-116 cells: **a** untreated, **b** curcumin treated, and **c** DX-CasCur-MC treated. The calculated parameters for untreated, curcumin-treated, and DX-CasCur-MC-treated HCT-116 cancer cells include % DNA damage (**d**), % DNA in tail (**e**), tail moment (**f**), and olive tail moment (**g**). Data is represented as mean ± SD (n = 3), the statistical significance difference in comparison with untreated cells is (*) ($p < 0.05$), (**) ($p < 0.01$), (***) ($p < 0.001$)

digestive gastric and intestinal fluids are depicted in Fig. 9a–c.

Upon a 1-h incubation in gastric fluid, a significant increase in DX-CasCur-MC size was observed, escalating from 255 to 3090 nm (Fig. 9b). This increase may be attributed to partial digestion of casein by pepsin, leading to the release of curcumin from leakage sites, as confirmed by the measured cumulative curcumin release of 23% (Shapira et al. 2012). Figure 9b suggests the potential for curcumin aggregation upon exposure to the gastric environment.

Subsequent incubation of DX-CasCur-MC in simulated intestinal fluid for 2 h results in a considerable reduction in nanoparticles size to 255 nm (Fig. 9b). Moreover, the percentage of released curcumin reaches approximately 69% (Fig. 9c). These outcomes highlight the stability of the proposed nanocomplex DX-CasCur-MC in simulated gastric fluid, attributed to the dual effects of methyl cellulose and dextran. These components prevent the premature release of curcumin in the stomach (23%), presenting a novel oral drug delivery system for curcumin (Luo et al. 2015). Furthermore, the increased amount of released curcumin in simulated intestinal fluid indicates the gradual breakdown of the nanocomplex in the intestinal

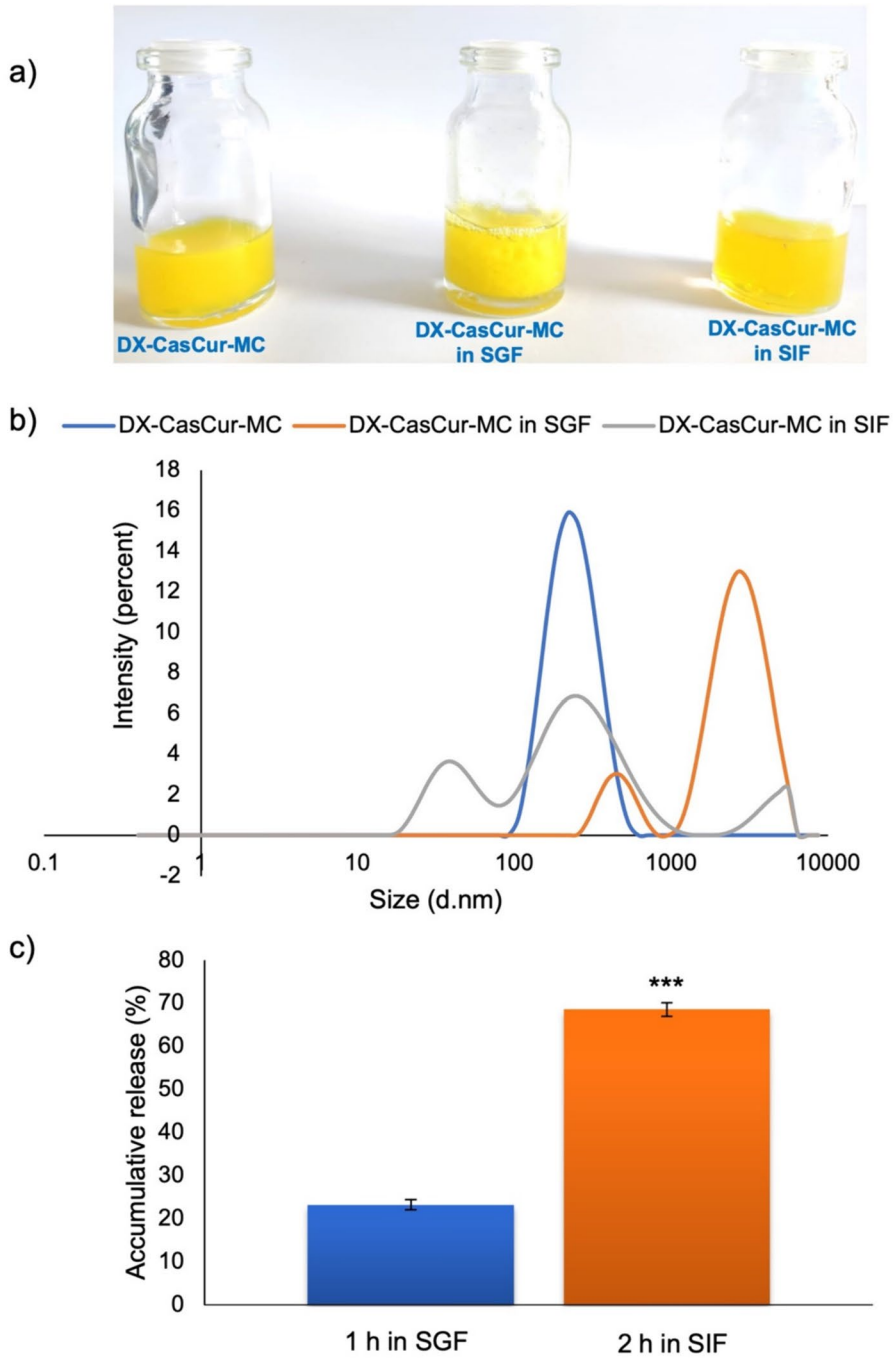

Fig. 9 In vitro release in simulated fluids: **a** An image of the behaviour of DX-CasCur-MC before and after incubation with digestive enzymes. **b** Size of DX-CasCur-MC nanoparticles in simulated gastric fluid (1 h) and simulated intestinal fluid (2 h). **c** Cumulative release percentage of curcumin in simulated gastric fluid (2 h) and simulated intestinal fluid (2 h). Data is represented as mean ± SD (n = 3)

environment, facilitating the entry of curcumin into the bloodstream.

In vivo study

Tumor growth inhibition study

Preclinical evaluation for the oral therapeutic effectiveness of DX-CasCur-MC against Ehrlich carcinoma was assessed in tumor bearing mice. The study based on comparing the impact of both curcumin-encapsulated dextran-casein-methyl cellulose nanoparticles and free curcumin on Ehrlich solid tumors in a mouse model, post five oral doses within 15-d period. The results, depicted in Fig. 10a, indicated a significant regression in tumor volume for the DX-CasCur-MC treated group compared to both the untreated and curcumin-treated groups.

Additionally, there was no significant change in mice body weight by the end of the experiment indicating the safety of the proposed nanoformulation, (Fig. 10b). Furthermore, the toxicity and biosafety issue was evaluated by the biochemical analysis of liver and kidney functions. A selected parameters including aspartate transaminase (AST), alanine transaminase (ALT), creatinine and urea for the two treated groups were measured and compared with untreated mice (S1).

The therapeutic efficacy of DX-CasCur-MC was evaluated in terms of measuring tumor weight at the end of the experiment. The dissected tumors from each group were collected and weighted. As illustrated in Fig. 10c, there was a notable reduction in tumor weight in DX-CasCur-MC treated group compared to both the curcumin-treated and untreated groups ($p < 0.001$).

As depicted in Fig. 10a–c, DX-CasCur-MC nanocomplex fabricated from natural materials significantly inhibited tumor growth in comparison with free curcumin. This is owed to many reasons including: (1) the successful oral delivery of curcumin to the small intestine overcoming the gastric barrier, (2) the amount of curcumin released (69%) in intestinal environment can safely absorbed in blood circulation, and (3) prolonged the circulation time of curcumin enabling better therapeutic effectiveness over free curcumin.

Histopathology examination

Histopathological examination of tumor sections, presented in Fig. 10d, provided further insights on the induction of cancer cell death. DX-CasCur-MC treated tumors exhibited extensive necrotic areas, indicating a substantial impact on tumor tissue. In contrast, the curcumin-treated tumors displayed a solid aggregation of neoplastic cells with minimal necrosis. The untreated tumor sections showed clusters of tumor cells with nearly no necrosis. These in vivo results collectively affirm the ability of DX-Cas-MC to facilitate oral delivery of curcumin, enhancement in its bioavailability, and induced cancer cell death.

Conclusion

In this study, we innovatively synthesized a nanocomplex consisting of casein, conjugated with the two polysaccharides methyl cellulose and dextran, specifically for the encapsulation of curcumin (DX-CasCur-MC). The physicochemical characterization of the nanocomplex indicated the successful conjugation of protein and polysaccharides with distinctive properties. The proposed DX-CasCur-MC demonstrated high curcumin encapsulation efficiency (92%) with a controlled and sustained drug release in physiological and tumor environments, vital for targeted drug delivery. The nanocomplex was able to enhance curcumin's potent anticancer property against the HCT-116 cancer cell line by perturbing cancer cell cycle and inducing cytotoxicity. Moreover, DX-CasCur-MC promoted substantial DNA damage and cellular autophagy in comparison with free curcumin. DX-CasCur-MC nanocomplex maintained its integrity in gastric fluid, controlling the release of curcumin, while facilitating its release in intestinal fluid. This confirms the suitability of DX-CasCur-MC for oral curcumin delivery. In vivo results highlighted the oral therapeutic efficacy of DX-CasCur-MC in terms of the significant inhibition of tumor growth relative to untreated and curcumin treated tumors. Hence, this indicates the potential of the DX-CasCur-MC nanocomplex to orally deliver curcumin to the tumor site with enhanced protection, thereby amplifying its anticancer activity compared to free curcumin.

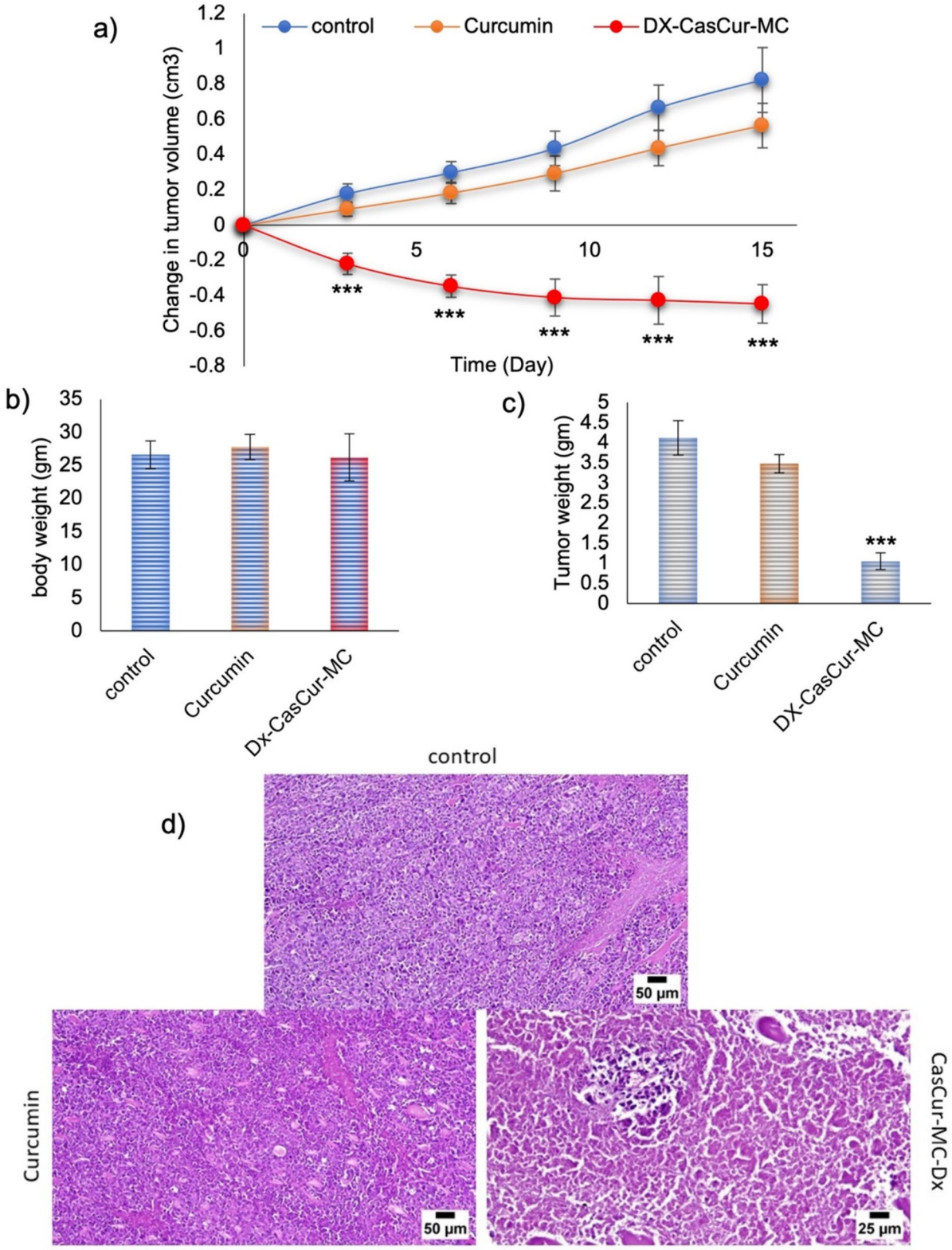
a)
control
Curcumin
DX-CasCur-MC
Change in tumor volume (cm3)
Time (Day)
***
b)
body weight (gm)
control
Curcumin
Dx-CasCur-MC
c)
Tumor weight (gm)
control
Curcumin
DX-CasCur-MC
d)
control
Curcumin
CasCur-MC-Dx
50 µm
50 µm
25 µm

◂**Fig. 10** In vivo evaluation of therapeutic efficacy of curcumin encapsulated in DX-Cas-MC and free curcumin (oral 5 doses/15 d) against Ehrlich carcinoma, **a** Monitoring tumor regression volume at predetermined time points. **b** Measurement of mice body weight at the experiment end point., **c** Tumor weight for the three experiment groups at the end of the experiment (15 d). Data is represented as mean ± SD (n = 3), the statistical significance difference in comparison with untreated cells is (*) ($p < 0.05$), (**) ($p < 0.01$), (***) ($p < 0.001$). **d** Histopathological examination of H&E-stained tumor sections dissected upon experiment termination

Acknowledgments This research work was funded by the Institutional Fund Projects under grant no. (IFPHI-734 247-1443). The authors gratefully acknowledge technical and financial support provided by the Ministry of Education and King Abdulaziz University, DSR, Jeddah, Saudi Arabia. The authors greatly appreciate Prof. Dr. Aml Hareedy, Faculty of Medicine, Cairo University for her kind contribution in histopathological examination of tumor sections.

Author contributions Samia F. Aboushoushah: project administration, funding acquisition, review and editing. Sans F. Abaza: resources, formal analysis and data curation. Nihal S. Elbialy: conceptualization, visualization, writing original draft, and final revision. Noha Mohamed: conceptualization, methodology, formal analysis, investigation, data curation.

Funding This work was supported by King Abdulaziz University- Institutional Funding Program for Research and Development- Ministry of Education, under grant no. (IFPHI-734-247-1443).

Data availability No datasets were generated or analysed during the current study.

Declarations

Conflict of interest The authors have not disclosed any competing interests.

Ethical approval The experiment received approval from Cairo University's Institutional Animal Care and Use Committee (CU-IACUC) (Egypt) under the reference CU-I-F-71-22. All experimental procedures adhered to CU-IACUC standards, following guidelines from the Council for International Organization of Medical Sciences and the International Council for Laboratory Animal Science (CIOMS/ICLAS, 2012), as well as the American Guide of Animal Care and Use. The study was reported in accordance with ARRIVE guidelines.

References

Abdel-Sattar OE, Allam RM, Al-Abd AM, El-Halawany AM, EL-Desoky AM, Mohamed SO, Sweilam SH, Khalid M, Abdel-Sattar E, Meselhy MR (2023) Hypophyllanthin and phyllanthin from *Phyllanthus niruri* synergize doxorubicin anticancer properties against resistant breast cancer cells. ACS Omega 8(31):28563–28576. https://doi.org/10.1021/ACSOMEGA.3C02953

Alavi F, Emam-Djomeh Z, Yarmand MS, Salami M, Momen S, Moosavi-Movahedi AA (2018) Cold gelation of curcumin loaded whey protein aggregates mixed with k-carrageenan: impact of gel microstructure on the gastrointestinal fate of curcumin. Food Hydrocoll 85:267–280. https://doi.org/10.1016/J.FOODHYD.2018.07.012

Anand P, Kunnumakkara AB, Newman RA, Aggarwal BB (2007) Bioavailability of curcumin: problems and promises. Mol Pharm 4(6):807–818. https://doi.org/10.1021/MP700113R

Araiza-Calahorra A, Akhtar M, Sarkar A (2018) Recent advances in emulsion-based delivery approaches for curcumin: from encapsulation to bioaccessibility. Trends Food Sci Technol 71:155–169. https://doi.org/10.1016/J.TIFS.2017.11.009

Ashrafizadeh M, Zarrabi A, Hashemi F, Moghadam ER, Hashemi F, Entezari M, Hushmandi K, Mohammadinejad R, Najafi M (2020) Curcumin in cancer therapy: a novel adjunct for combination chemotherapy with paclitaxel and alleviation of its adverse effects. Life Sci. https://doi.org/10.1016/J.LFS.2020.117984

Began G, Sudharshan E, Udaya Sanka K, Appu Rao AG (1999) Interaction of curcumin with phosphatidylcholine: a spectrofluorometric study. J Agric Food Chem 47(12):4992–4997. https://doi.org/10.1021/JF9900837

Beltzig L, Frumkina A, Schwarzenbach C, Kaina B (2021) Cytotoxic, genotoxic and senolytic potential of native and micellar curcumin. Nutrients. https://doi.org/10.3390/NU13072385

Benzaria A, Maresca M, Taieb N, Dumay E (2013) Interaction of curcumin with phosphocasein micelles processed or not by dynamic high-pressure. Food Chem 138(4):2327–2337. https://doi.org/10.1016/J.FOODCHEM.2012.12.017

Bich VT, Thuy NT, Binh NT, Huong NTM, Yen PND, Luong TT (2009) Structural and spectral properties of curcumin and metal- curcumin complex derived from turmeric (*Curcuma longa*). In: Proceedings in Physics, vol 127. Springer, pp 271–278. https://doi.org/10.1007/978-3-540-88201-5_31

Blume-Jensen P, Hunter T (2001) Oncogenic kinase signalling. Nature 411(6835):355–365. https://doi.org/10.1038/35077225

Bortel N, Armeanu-Ebinger S, Schmid E, Kirchner B, Frank J, Kocher A, Schiborr C, Warmann S, Fuchs J, Ellerkamp V (2015) Effects of curcumin in pediatric epithelial liver tumors: inhibition of tumor growth and alpha-fetoprotein in vitro and in vivo involving the NFkappaB- and the beta-catenin pathways. Oncotarget 6(38):40680. https://doi.org/10.18632/ONCOTARGET.5673

Bray F, Ferlay J, Soerjomataram I, Siegel RL, Torre LA, Jemal A (2018) Global cancer statistics 2018: GLOBOCAN estimates of incidence and mortality worldwide for 36 cancers in 185 countries. CA Cancer J Clin 68(6):394–424. https://doi.org/10.3322/caac.21492

Chang C, Wang T, Hu Q, Luo Y (2017) Caseinate-zein-polysaccharide complex nanoparticles as potential oral

delivery vehicles for curcumin: effect of polysaccharide type and chemical cross-linking. Food Hydrocoll 72:254–262. https://doi.org/10.1016/J.FOODHYD.2017.05.039

Chau Y, Padera RF, Dang NM, Langer R (2006) Antitumor efficacy of a novel polymer-peptide-drug conjugate in human tumor xenograft models. Int J Cancer 118(6):1519–1526. https://doi.org/10.1002/IJC.21495

Chen L, Subirade M (2005) Chitosan/beta-lactoglobulin core-shell nanoparticles as nutraceutical carriers. Biomaterials 26(30):6041–6053. https://doi.org/10.1016/J.BIOMATERIALS.2005.03.011

Chen L, Wei J, An M, Zhang L, Lin S, Shu G, Yuan Z, Lin J, Peng G, Liang X, Yin L, Zhang W, Zhao L, Fu H (2020) Casein nanoparticles as oral delivery carriers of mequindox for the improved bioavailability. Colloids Surf B Biointerfaces. https://doi.org/10.1016/J.COLSURFB.2020.111221

Chen L, He Y, Zhu J, Zhao S, Qi S, Chen X, Zhang H, Ni Z, Zhou Y, Chen G, Liu S, Xie T (2023) The roles and mechanism of m6A RNA methylation regulators in cancer immunity. Biomed Pharmacother. https://doi.org/10.1016/J.BIOPHA.2023.114839

Chen Y, Cai S, He N, Huang X, Hong Z, He J, Chen H, Zhang Y (2024) An effective method to prepare curcumin-loaded soy protein isolate nanoparticles co-stabilized by carrageenan and fucoidan. Pharmaceuticals. https://doi.org/10.3390/PH17040534

Choi KY, Saravanakumar G, Park JH, Park K (2012) Hyaluronic acid-based nanocarriers for intracellular targeting: interfacial interactions with proteins in cancer. Colloids Surf B Biointerfaces 99:82–94. https://doi.org/10.1016/J.COLSURFB.2011.10.029

Deb VK, Chauhan N, Chandra R, Jain U (2024) Recent progression in controlled drug delivery through advanced functional nanomaterials in cancer therapy. BioNanoScience 2024:1–44. https://doi.org/10.1007/S12668-023-01297-6

Ding L, Huang Y, Cai XX, Wang S (2019) Impact of pH, ionic strength and chitosan charge density on chitosan/casein complexation and phase behavior. Carbohydr Polym 208:133–141. https://doi.org/10.1016/J.CARBPOL.2018.12.015

Elbialy NS, Mohamed N (2020) Alginate-coated caseinate nanoparticles for doxorubicin delivery: preparation, characterisation, and in vivo assessment. Int J Biol Macromol 154:114–122. https://doi.org/10.1016/J.IJBIOMAC.2020.03.027

Elzoghby AO, Abo El-Fotoh WS, Elgindy NA (2011) Casein-based formulations as promising controlled release drug delivery systems. J Control Release 153(3):206–216. https://doi.org/10.1016/J.JCONREL.2011.02.010

Fan Q, Ma J, Xu Q, Zhang J, Simion D, Carmen G, Guo C (2015) Animal-derived natural products review: focus on novel modifications and applications. Colloids Surf B Biointerfaces 128:181–190. https://doi.org/10.1016/J.COLSURFB.2015.02.033

Fan Y, Yi J, Zhang Y, Yokoyama W (2018) Fabrication of curcumin-loaded bovine serum albumin (BSA)-dextran nanoparticles and the cellular antioxidant activity. Food Chem 239:1210–1218. https://doi.org/10.1016/J.FOODCHEM.2017.07.075

Gao TH, Liao W, Lin LT, Zhu ZP, Lu MG, Fu CM, Xie T (2022) Curcumae rhizoma and its major constituents against hepatobiliary disease: pharmacotherapeutic properties and potential clinical applications. Phytomedicine. https://doi.org/10.1016/J.PHYMED.2022.154090

Gaucher G, Dufresne MH, Sant VP, Kang N, Maysinger D, Leroux JC (2005) Block copolymer micelles: preparation, characterization and application in drug delivery. J Control Release 109(1–3):169–188. https://doi.org/10.1016/J.JCONREL.2005.09.034

Ghobadi-Oghaz N, Asoodeh A, Mohammadi M (2022) Fabrication, characterization and in vitro cell exposure study of zein-chitosan nanoparticles for co-delivery of curcumin and berberine. Int J Biol Macromol 204:576–586. https://doi.org/10.1016/J.IJBIOMAC.2022.02.041

Guan F, Ding Y, Zhang Y, Zhou Y, Li M, Wang C (2016) Curcumin suppresses proliferation and migration of MDA-MB-231 breast cancer cells through autophagy-dependent AKT degradation. PLoS ONE 11(1):e0146553. https://doi.org/10.1371/JOURNAL.PONE.0146553

Gupta A, Keddie DJ, Kannappan V, Gibson H, Khalil IR, Kowalczuk M, Martin C, Shuai X, Radecka I (2019) Production and characterisation of bacterial cellulose hydrogels loaded with curcumin encapsulated in cyclodextrins as wound dressings. Eur Polym J 118:437–450. https://doi.org/10.1016/J.EURPOLYMJ.2019.06.018

Hao X, Han S, Qin D, Zhang Y, Jin P, Du Q (2021) Superior anti-infective potential of eugenol–casein nanoparticles combined with polyethylene glycol against *Colletotrichum musae* infections. RSC Adv 11(8):4646. https://doi.org/10.1039/D0RA09283E

He X, Jiang Z, Akakuru OU, Li J, Wu A (2021) Nanoscale covalent organic frameworks: from controlled synthesis to cancer therapy. Chem Commun 57(93):12417–12435. https://doi.org/10.1039/D1CC04846E

He Z, Yue C, Chen X, Li X, Zhang L, Tan S, Yi X, Luo G, Zhou Y (2023) Integrative analysis identified CD38 as a key node that correlates highly with immunophenotype, chemoradiotherapy resistance, and prognosis of head and neck cancer. J Cancer 14(1):72–87. https://doi.org/10.7150/JCA.59730

Ho NAD, Leo CP (2021) A review on the emerging applications of cellulose, cellulose derivatives and nanocellulose in carbon capture. Environ Res. https://doi.org/10.1016/J.ENVRES.2021.111100

Jiang T, Feng L, Zheng X (2012) Effect of chitosan coating enriched with thyme oil on postharvest quality and shelf life of shiitake mushroom (*Lentinus edodes*). J Agric Food Chem 60(1):188–196. https://doi.org/10.1021/JF202638U

Jin P, Yao R, Qin D, Chen Q, Du Q (2019) Enhancement in antibacterial activities of eugenol-entrapped ethosome nanoparticles via strengthening its permeability and sustained release. J Agric Food Chem 67(5):1371–1380. https://doi.org/10.1021/ACS.JAFC.8B06278

Kasi PD, Tamilselvam R, Skalicka-Woźniak K, Nabavi SF, Daglia M, Bishayee A, Pazoki-Toroudi H, Nabavi SM (2016) Molecular targets of curcumin for cancer therapy: an updated review. Tumour Biol 37(10):13017–13028. https://doi.org/10.1007/S13277-016-5183-Y

Keshavarz M, Saeidifar M, Nasab NA, Safa O, Nikoofal-Sahlabadi S (2023) Curcumin derivative loaded albumin

nanoparticles: preparation, molecular interaction study and evaluation of physicochemical properties, in-vitro release and cytotoxicity. Nanomed Res J 8(1):69–88. https://doi.org/10.22034/NMRJ.2023.01.007

Khadem Sadigh M, Zakerhamidi MS, Shamkhali AN, Babaei E (2017) Photo-physical behaviors of various active forms of curcumin in polar and low polar environments. J Photochem Photobiol A Chem 348:188–198. https://doi.org/10.1016/J.JPHOTOCHEM.2017.08.050

Klemm D, Petzold-Welcke K, Kramer F, Richter T, Raddatz V, Fried W, Nietzsche S, Bellmann T, Fischer D (2021) Biotech nanocellulose: a review on progress in product design and today's state of technical and medical applications. Carbohydr Polym. https://doi.org/10.1016/J.CARBPOL.2020.117313

Li J, Chen Z (2022) Fabrication of heat-treated soybean protein isolate-EGCG complex nanoparticle as a functional carrier for curcumin. LWT 159:113059. https://doi.org/10.1016/J.LWT.2021.113059

Li J, Wang X (2015) Binding of (-)-epigallocatechin-3-gallate with thermally-induced bovine serum albumin/ι-carrageenan particles. Food Chem 168:566–571. https://doi.org/10.1016/J.FOODCHEM.2014.07.097

Li NN, Fu CP, Zhang LM (2014) Using casein and oxidized hyaluronic acid to form biocompatible composite hydrogels for controlled drug release. Mater Sci Eng C Mater Biol Appl 36(1):287–293. https://doi.org/10.1016/J.MSEC.2013.12.025

Li K, Zhang Y, Hao X, Xie D, Wang C, Zhang H, Jin P, Du Q (2022a) Improved stability and in vitro anti-arthritis bioactivity of curcumin-casein nanoparticles by ultrasound-driven encapsulation. Nutrients. https://doi.org/10.3390/NU14235192

Li M, Xiao Y, Liu M, Ning Q, Xiang Z, Zheng X, Tang S, Mo Z (2022b) MiR-26a-5p regulates proliferation, apoptosis, migration and invasion via inhibiting hydroxysteroid dehydrogenase like-2 in cervical cancer cell. BMC Cancer. https://doi.org/10.1186/S12885-022-09970-X

Lin TP, Huang AC, Wei HC, Lin JG, Chung JG (2007) Ethyl 2-[N-p-chlorobenzyl-(2′-methyl)] anilino-4-oxo-4,5-dihydrofuran-3-carboxylate (JOT01007) induces apoptosis in human cervical cancer Ca ski cells. In Vivo (Brooklyn) 21(2):397–406

Liu Y, Guo R (2008) pH-dependent structures and properties of casein micelles. Biophys Chem 136(2–3):67–73. https://doi.org/10.1016/J.BPC.2008.03.012

Liu C, Jiang TT, Yuan ZX, Lu Y (2020) Self-assembled casein nanoparticles loading triptolide for the enhancement of oral bioavailability. Nat Prod Commun. https://doi.org/10.1177/1934578X20948352

Liu K, Jiang Z, Lalancette RA, Tang X, Jäkle F (2022a) Near-infrared-absorbing B-N Lewis pair-functionalized anthracenes: electronic structure tuning, conformational isomerism, and applications in photothermal cancer therapy. J Am Chem Soc 144(41):18908–18917. https://doi.org/10.1021/JACS.2C06538

Liu K, Jiang Z, Zhao F, Wang W, Jäkle F, Wang N, Tang X, Yin X, Chen P (2022b) Triarylboron-doped acenethiophenes as organic sonosensitizers for highly efficient sonodynamic therapy with low phototoxicity. Adv Mater. https://doi.org/10.1002/ADMA.202206594

Liu L, Yang S, Chen F, Cheng KW (2022c) Polysaccharide-zein composite nanoparticles for enhancing cellular uptake and oral bioavailability of curcumin: characterization, anti-colorectal cancer effect, and pharmacokinetics. Front Nutr. https://doi.org/10.3389/FNUT.2022.846282

Low LE, Tan LTH, Goh BH, Tey BT, Ong BH, Tang SY (2019) Magnetic cellulose nanocrystal stabilized pickering emulsions for enhanced bioactive release and human colon cancer therapy. Int J Biol Macromol 127:76–84. https://doi.org/10.1016/J.IJBIOMAC.2019.01.037

Luo Y, Zhang B, Whent M, Yu LL, Wang Q (2011) Preparation and characterization of zein/chitosan complex for encapsulation of α-tocopherol, and its in vitro controlled release study. Colloids Surf B Biointerfaces 85(2):145–152. https://doi.org/10.1016/J.COLSURFB.2011.02.020

Luo Y, Pan K, Zhong Q (2015) Casein/pectin nanocomplexes as potential oral delivery vehicles. Int J Pharm 486(1–2):59–68. https://doi.org/10.1016/J.IJPHARM.2015.03.043

Mansoori B, Mohammadi A, Davudian S, Shirjang S, Baradaran B (2017) The different mechanisms of cancer drug resistance: a brief review. Adv Pharm Bull 7(3):339. https://doi.org/10.15171/APB.2017.041

Naksuriya O, Okonogi S, Schiffelers RM, Hennink WE (2014) Curcumin nanoformulations: a review of pharmaceutical properties and preclinical studies and clinical data related to cancer treatment. Biomaterials 35(10):3365–3383. https://doi.org/10.1016/J.BIOMATERIALS.2013.12.090

Noble MEM, Endicott JA, Johnson LN (2004) Protein kinase inhibitors: insights into drug design from structure. Science 303(5665):1800–1805. https://doi.org/10.1126/SCIENCE.1095920

Oliveira RL, Vieira JG, Barud HS, Assunção RMN, Filho GR, Ribeiro SJL, Messadeqq Y (2015) Synthesis and characterization of methylcellulose produced from bacterial cellulose under heterogeneous condition. J Braz Chem Soc 26(9):1861–1870. https://doi.org/10.5935/0103-5053.20150163

Pan L, Feng F, Wu J, Fan S, Han J, Wang S, Yang L, Liu W, Wang C, Xu K (2022) Demethylzeylasteral targets lactate by inhibiting histone lactylation to suppress the tumorigenicity of liver cancer stem cells. Pharmacol Res. https://doi.org/10.1016/J.PHRS.2022.106270

Popat A, Karmakar S, Jambhrunkar S, Xu C, Yu C (2014) Curcumin-cyclodextrin encapsulated chitosan nanoconjugates with enhanced solubility and cell cytotoxicity. Colloids Surf B Biointerfaces 117:520–527. https://doi.org/10.1016/J.COLSURFB.2014.03.005

Posey JA, Saif MW, Carlisle R, Goetz A, Rizzo J, Stevenson S, Rudoltz MS, Kwiatek J, Simmons P, Rowinsky EK, Takimoto CH, Tolcher AW (2005) Phase 1 study of weekly polyethylene glycol-camptothecin in patients with advanced solid tumors and lymphomas. Clin Cancer Res 11(21):7866–7871. https://doi.org/10.1158/1078-0432.CCR-05-0783

Pradhan D, Biswasroy P, Sahu A, Sahu DK, Ghosh G, Rath G (2021) Recent advances in herbal nanomedicines for cancer treatment. Curr Mol Pharmacol 14(3):292–305. https://doi.org/10.2174/1874467213666200525010624

Prusty K, Swain SK (2019) Release of ciprofloxacin drugs by nano gold embedded cellulose grafted polyacrylamide

hybrid nanocomposite hydrogels. Int J Biol Macromol 126:765–775. https://doi.org/10.1016/J.IJBIOMAC.2018.12.258

Rajendran S, Ravi SN, Nair VM, Sree RP, Packirisamy ASB, Palanivelu J (2024) Recent development and future aspects: nano-based drug delivery system in cancer therapy. Top Catal 67(1):203–217. https://doi.org/10.1007/S11244-023-01893-6

Rauf A, Imran M, Butt MS, Nadeem M, Peters DG, Mubarak MS (2018) Resveratrol as an anti-cancer agent: a review. Crit Rev Food Sci Nutr 58(9):1428–1447. https://doi.org/10.1080/10408398.2016.1263597

Sala de Oyanguren FJ, Rainey NE, Moustapha A, Saric A, Sureau F, O'Connor JE, Petit PX (2020) Highlighting curcumin-induced crosstalk between autophagy and apoptosis as supported by its specific subcellular localization. Cells. https://doi.org/10.3390/CELLS9020361

Schneible JD, Daniele MA, Menegatti S (2021) Natural and synthetic biopolymers in drug delivery and tissue engineering. Biopolym Biomed Biotechnol Appl. https://doi.org/10.1002/9783527818310.CH9

Shapira A, Davidson I, Avni N, Assaraf YG, Livney YD (2012) β-Casein nanoparticle-based oral drug delivery system for potential treatment of gastric carcinoma: stability, target-activated release and cytotoxicity. Eur J Pharm Biopharm 80(2):298–305. https://doi.org/10.1016/J.EJPB.2011.10.022

Shehzad A, Wahid F, Lee YS (2010) Curcumin in cancer chemoprevention: molecular targets, pharmacokinetics, bioavailability, and clinical trials. Arch Pharm 343(9):489–499. https://doi.org/10.1002/ARDP.200900319

Shen W, Pei P, Zhang C, Li J, Han X, Liu T, Shi X, Su Z, Han G, Hu L, Yang K (2023) A polymeric hydrogel to eliminate programmed death-ligand 1 for enhanced tumor radio-immunotherapy. ACS Nano 17(23):23998–24011. https://doi.org/10.1021/ACSNANO.3C08875

Shukla R, Shukla S, Bivolarski V, Iliev I, Ivanova I, Goyal A (2011) Structural characterization of insoluble dextran produced by *Leuconostoc mesenteroides* NRRL B-1149 in the presence of maltose. Food Technol Biotechnol 49(3):291–296

Siegel RL, Miller KD, Jemal A (2020) Cancer statistics. CA Cancer J Clin 70(1):7–30. https://doi.org/10.3322/CAAC.21590

Sun X, Wang H, Li S, Song C, Zhang S, Ren J, Udenigwe CC (2022) Maillard-type protein-polysaccharide conjugates and electrostatic protein-polysaccharide complexes as delivery vehicles for food bioactive ingredients: formation, types, and applications. Gels. https://doi.org/10.3390/GELS8020135

Vandamme ThF, Lenourry A, Charrueau C, Chaumeil J-C (2002) The use of polysaccharides to target drugs to the colon. Carbohydr Polym 3(48):219–231

Wu Y, Wang X (2017) Binding, stability, and antioxidant activity of curcumin with self-assembled casein–dextran conjugate micelles. Int J Food Prop 20(12):3295–3307. https://doi.org/10.1080/10942912.2017.1286505

Xiao K, Jiang J, Guan C, Dong C, Wang G, Bai L, Sun J, Hu C, Bai C (2013) Curcumin induces autophagy via activating the AMPK signaling pathway in lung adenocarcinoma cells. J Pharmacol Sci 123(2):102–109. https://doi.org/10.1254/JPHS.13085FP

Xiaolong J (2023) Research progress on degradation methods and product properties of plant polysaccharides. J Light Ind 38(3):55

Xie Z (ed) (2021) Autophagy: biology and diseases, p 1208. https://doi.org/10.1007/978-981-16-2830-6

Xu G, Wang C, Yao P (2017) Stable emulsion produced from casein and soy polysaccharide compacted complex for protection and oral delivery of curcumin. Food Hydrocoll 71:108–117. https://doi.org/10.1016/J.FOODHYD.2017.05.010

Xu G, Li L, Bao X, Yao P (2020) Curcumin, casein and soy polysaccharide ternary complex nanoparticles for enhanced dispersibility, stability and oral bioavailability of curcumin. Food Biosci 35:100569. https://doi.org/10.1016/J.FBIO.2020.100569

Xu H, Li L, Wang S, Wang Z, Qu L, Wang C, Xu K (2023) Royal jelly acid suppresses hepatocellular carcinoma tumorigenicity by inhibiting H3 histone lactylation at H3K9la and H3K14la sites. Phytomedicine. https://doi.org/10.1016/J.PHYMED.2023.154940

Xv L, Qian X, Wang Y, Yu C, Qin D, Zhang Y, Jin P, Du Q (2020) Structural modification of nanomicelles through phosphatidylcholine: the enhanced drug-loading capacity and anticancer activity of celecoxib-casein nanoparticles for the intravenous delivery of celecoxib. Nanomaterials. https://doi.org/10.3390/NANO10030451

Yadav N, Parveen S, Banerjee M (2020) Potential of nano-phytochemicals in cervical cancer therapy. Clin Chim Acta 505:60–72. https://doi.org/10.1016/J.CCA.2020.01.035

Yallapu MM, Jaggi M, Chauhan SC (2013) Curcumin nanomedicine: a road to cancer therapeutics. Curr Pharm Des 19(11):1994–2010. https://doi.org/10.2174/138161213805289219

Yi J, Li L, Yin Z, Quan Y, Tan R, Chen S, Lang J, Li J, Zeng J, Li Y, Sun Z, Zhao J (2023) Polypeptide from moschus suppresses lipopolysaccharide-induced inflammation by inhibiting NF-κ B-ROS/NLRP3 pathway. Chin J Integr Med 29(10):895–904. https://doi.org/10.1007/S11655-023-3598-Z

Yuan Y, Li H, Zhu J, Liu C, Sun X, Wang D, Xu Y (2020) Fabrication and characterization of zein nanoparticles by dextran sulfate coating as vehicles for delivery of curcumin. Int J Biol Macromol 151:1074–1083. https://doi.org/10.1016/J.IJBIOMAC.2019.10.149

Zhang L, Shi H, Tan X, Jiang Z, Wang P, Qin J (2022) Ten-gram-scale mechanochemical synthesis of ternary lanthanum coordination polymers for antibacterial and antitumor activities. Front Chem. https://doi.org/10.3389/FCHEM.2022.898324

Zhang Y, Wang D, Tan D, Zou A, Wang Z, Gong H, Yang Y, Sun L, Lin X, Liang M, Yu Y, He X, Yu G, Wang W, Cai C (2024) Immune-enhancing activity of compound polysaccharide on the inactivated influenza vaccine. Carbohydr Polym. https://doi.org/10.1016/J.CARBPOL.2024.122080

Zheng B, Zhang Z, Chen F, Luo X, Mcclements DJ (2017) Impact of delivery system type on curcumin stability: Comparison of curcumin degradation in aqueous

solutions, emulsions, and hydrogel 2 beads. Food Hydrocoll 71:187
Zoi V, Galani V, Lianos GD, Voulgaris S, Kyritsis AP, Alexiou GA (2021) The role of curcumin in cancer treatment. Biomedicines. https://doi.org/10.3390/BIOMEDICINES9091086